Title: LKB1 regulates JNK-dependent stress signaling and apoptotic dependency of *KRAS*-mutant lung cancers

Authors:
Chendi Li[1, 2], Mohammed Usman Syed[1], Anahita Nimbalkar[1], Yi Shen[1], Cameron Fraser[3-5], Zintis Inde[3-5], Xingping Qin[3-5], Jian Ouyang[1], Johannes Kreuzer[1], Sarah E. Clark[1], Grace Kelley[1], Emily Hensley[1], Robert Morris[1], Raul Lazaro[7], Brian Belmontes[7], Audris Oh[1], Makeba Walcott[1], Christopher Nabel[1,8], Sean Caenepeel[7], Anne Y. Saiki[7], Karen Rex[7], J. Russell Lipford[7], Rebecca S. Heist[1,2], Jessica J. Lin[1,2], Wilhelm Haas[1], Kristopher Sarosiek[3-6], Paul E. Hughes[7], Aaron N. Hata[1,2].

Affiliations:
[1]Massachusetts General Hospital Cancer Center, Charlestown, Massachusetts.
[2]Department of Medicine, Massachusetts General Hospital and Harvard Medical School, Boston, Massachusetts.
[3]John B. Little Center for Radiation Sciences, Harvard T.H. Chan School of Public Health, Boston, Massachusetts.
[4]Molecular and Integrative Physiological Sciences Program, Harvard T.H. Chan School of Public Health, Boston, Massachusetts.
[5]Lab for Systems Pharmacology, Harvard Medical School, Boston, Massachusetts.
[6]Department of Medical Oncology, Dana-Farber Cancer Institute/ Harvard Cancer Center; Boston MA.
[7]Amgen Research, Amgen Inc., Thousand Oaks, California
[8]Massachusetts Institute of Technology, Cambridge, Massachusetts.

Corresponding Author:
Aaron N. Hata, MD, PhD, Massachusetts General Hospital Cancer Center, 149 13th Street, Charlestown, MA 02129. Phone: 617-724-3442; E-mail: ahata@mgh.harvard.edu

Abstract

The efficacy of molecularly targeted anti-cancer therapies may be limited by the presence of co-occurring mutations within a tumor[1-3]. Conversely, these alterations may confer collateral vulnerabilities that can be leveraged for the development of novel therapeutic approaches. *KRAS*-mutant lung cancers are distinguished by recurrent inactivating mutations in the tumor suppressor *STK11*/LKB1[4] that facilitate tumorigenesis by modulating energy balance[5,6] , enhancing metastatic potential[7,8] and enabling immune evasion[9,10]. However, whether LKB1 plays a role in modulating cellular responses to therapeutic stress is largely unknown. Here we show that LKB1 suppresses JNK-dependent stress signaling in *KRAS*-mutant lung cancer cells upon acute loss of oncogenic signaling. In LKB1-deficient *KRAS*-mutant cells, inhibition of KRAS or its downstream effector MEK leads to hyperactivation of JNK due to loss of NUAK-mediated PP1B phosphatase activity. JNK-mediated inhibitory phosphorylation of BCL-XL rewires apoptotic dependencies, rendering LKB1-deficient cells vulnerable to MCL-1 inhibition. These results uncover a previously unknown role for LKB1 in regulating stress signaling and the mitochondrial apoptotic response of cancer cells independent of its tumor suppressor activity mediated by AMPK[11-13] and SIK[14,15] kinases. Additionally, our study reveals a therapy-induced vulnerability in LKB1-deficient *KRAS*-mutant lung cancer cells that could be exploited as a genotype-informed strategy to improve the efficacy of KRAS-targeted therapies.

Main Text

Mutations in KRAS, a small GTPase that regulates MAPK/ERK signaling, define the largest genetically-defined subset of non-small cell lung cancer, representing 25-30% of all lung adenocarcinomas[16]. The recent US FDA and European Commission approvals of sotorasib (AMG 510)[17] and adagrasib (MRTX849)[18], small molecule covalent $KRAS^{G12C}$-selective inhibitors, marked a milestone in the development of targeted therapies for *KRAS*-mutant cancers. While most NSCLC patients treated with sotorasib experience clinical benefit, only ~40% achieve a partial response[19]. To improve efficacy, drug combination strategies that target mechanisms of adaptive resistance[20-23] or immune evasion (NCT04613596, NCT06119581) are being tested in the clinic. *KRAS*-mutant lung cancers harbor diverse co-occurring alterations such as *STK11*/LKB1 loss and *KEAP1* mutations[16] that may contribute to lack of response to different therapies including anti-PD-(L)1 immune checkpoint inhibitors[9] and $KRAS^{G12C}$ inhibitors[19,18]. However, whether co-occurring alterations induce vulnerabilities that can be therapeutically exploited in a genotype-directed manner remains largely undefined.

To investigate the impact of common co-occurring genomic alterations on $KRAS^{G12C}$ inhibitor combination strategies targeting distinct pathways, we screened a panel of $KRAS^{G12C}$-mutant NSCLC cell lines harboring diverse co-occurring mutations (Fig. S1A) with sotorasib alone or in combination with inhibitors targeting SHP2 (TNO155), CDK4/6 (abemaciclib), PI3K (GDC-0941), BCL-XL/BCL-2 (navitoclax) or MCL-1 (AMG 176) (Fig. 1A). Consistent with prior studies of $KRAS^{G12C}$ inhibitors[17,22,24,25], we observed varying sensitivity to single-agent $KRAS^{G12C}$ inhibition, which was independent of the most common co-occurring mutations such as *TP53*, *STK11*/LKB1 and *KEAP1* (Fig. S1B-C; Sup. Table 1). To quantify the efficacy of $KRAS^{G12C}$ combinations compared to $KRAS^{G12C}$ alone, we calculated the relative change in AUC (e.g., the area between the single agent and combination dose response curves, normalized to the effect of sotorasib alone), referred to hereafter as simply ΔAUC (Fig. S1D). As expected, combining sotorasib with other inhibitors led to greater suppression of cell viability

than single-agent sotorasib in most cell lines, although the effect was variable (Fig. S1E). Whereas the presence of co-occurring mutations had little impact on sensitivity to combinations targeting SHP2, CDK4/6 or BCL-XL/BCL-2, cell lines with co-occurring mutations or loss of *STK11*/LKB1 were more sensitive to combinations targeting MCL-1 or PI3K (Fig. 1B-C, Fig. S1E). PI3K inhibition can effect diverse cellular changes in oncogene-addicted cancers, including mTOR-dependent down-regulation of MCL-1 protein levels[26,27], which we confirmed (Fig. S1F). To further the investigate the role of MCL-1 in a larger cohort of *KRAS*-mutant NSCLC cell lines that included *KRAS* mutations other than G12C, we tested the MEK inhibitor trametinib in combination with AMG 176 (or the related compound AM-8621[28]). Similarly, we observed greater activity of trametinib + AMG 176 in cell lines with LKB1 loss (Fig. 1D, S1G). We also confirmed these findings with additional MEK (cobimetinib) and $KRAS^{G12C}$ (adagrasib) inhibitors (Fig. S1H). The increase in combination activity resulted from modestly greater sensitivity of a subset of LKB1-deficient cell lines to single agent MCL-1 inhibition (Fig. S1I) as well synergistic activity between trametinib and AMG 176 (Fig. S2A), resulting in a net cytotoxic effect by the combination (Fig. S2B). LKB1-deficient cell lines with high ΔAUC values exhibited robust apoptosis upon combined inhibition of KRAS/MAPK and MCL-1, while the apoptotic response of LKB1 wild-type (WT) cell lines was minimal (Fig. 1E-F), suggesting that LKB1 may modulate apoptotic dependencies of *KRAS*-mutant lung cancers.

To determine whether LKB1 plays a causal role in tuning the apoptotic response of *KRAS*-mutant NSCLC cells, we restored LKB1 expression in LKB1-deficient cell lines or deleted LKB1 in WT cell lines (Fig. S3A). Re-expression of LKB1 decreased sensitivity to combined sotorasib or trametinib + MCL-1 inhibition, and conversely, CRISPR-mediated deletion of LKB1 sensitized LKB1 WT cells to sotorasib or trametinib + MCL-1 inhibition (Fig. 1G-H, S3C-D). Restoration or deletion of LKB1 did not alter the response to sotorasib alone (Fig. S3E) or alter cell proliferation rate (Fig. S3B), suggesting that the changes in sensitivity to the drug combination that occur upon gain or loss of LKB1 are mediated primarily by differences in MCL-1-dependent regulation of apoptosis. Consistent with this notion, restoration or deletion of LKB1 decreased or increased the apoptotic cell death to trametinib + AMG 176, respectively (Fig. 1I-J, S3F), with restoration of LKB1 expression converting cytoxic reponses to cytostatic responses (Fig. S3G). To confirm these results *in vivo*, we established isogenic H2030 EV and LKB1 xenograft tumors in mice. Similar to the *in vitro* results, restoration of LKB1 abolished tumor regression of H2030 xenograft tumors in response to sotorasib or trametinib + AMG 176 (Fig. 1K, S3H). Collectively, these results demonstrate that that loss of LKB1 sensitizes *KRAS*-mutant NSCLC cells to combined MAPK + MCL-1 inhibition both *in vitro* and *in vivo*.

LKB1 is a master serine/threonine kinase that regulates multiple cellular process including growth[12,29], cell metabolism[5,6] and cell polarity[30-32]. We hypothesized that loss of LKB1 rewires downstream kinase signaling networks to confer dependency on MCL-1, especially upon disruption of oncogenic signaling. Supporting this, expression of a kinase-dead $LKB1^{K781}$ (kd) mutant[11] did not rescue LKB1-deficient cells from combined MEK + MCL-1 inhibition (Fig. S4A-B), demonstrating that LKB1 catalytic activity is required for the observed difference in drug sensitivity. To identify differences in kinase signaling in *KRAS*-mutant NSCLC cells with or without LKB1, we performed mass spectrometry-based global phosphoproteome profiling[33] of isogenic H2030 (EV, LKB1 and LKB1-kd) and H358 (KO GFP, KO LKB1) cells before and after treatment with trametinib (Fig. 2A). We quantified 27364 unique phosphosites (Fig. S4C-D), then performed phosphosite signature analysis[34] to identify the kinases that were differentially activated in each of these contexts. Consistent with the known effect of MEK inhibition on cell cycle progression[35], we observed down-regulation of cell cycle associated phospho-signatures

including cyclin-dependent kinases, ATM, ATR, Aurora Kinase B, and PLK1 in response to trametinib treatment (Fig. S4E). In the absence of drug treatment, there were few statistically significant differences (and no overlap) in kinase signatures between LKB1 wild-type and deficient cells (Fig. S4F), likely a result of the nutrient-rich cell culture environment. To identify drug-induced differences in kinase activity regulated by LKB1, we looked for kinase phospho-signatures that were enriched in trametinib-treated LKB1-deficient cells relative to their wild-type counterparts (H2030 EV versus LKB1, H358 KO LKB1 versus KO GFP) but not enriched in H2030 EV versus kinase-dead LKB1^{K87I} cells. While several signatures were enriched in trametinib-treated LKB1-deficient cells for either isogenic pair, only one signature – c-Jun N-terminal kinase1 (JNK1) – satisfied these criteria (Fig. 2B). Specifically, the phosphorylation of well-established substrates of JNK1, such as ATF2, JUN and JUNB, increased to a greater extent in H2030 EV and H358 KO LKB1 cells after trametinib treatment compared to their LKB1 wild-type pairs. Next, we performed proteomic analysis of H2030 and H358 isogenic cells after treatment with trametinib + AMG 176. JNK phospho-signatures rapidly (8 hours) increased in H358 LKB1 KO cells compared to control cells, and a subset of JNK substrates showed increase phosphorylation in LKB1-deficient H2030 cells (Fig. S4G-H). These results suggest that LKB1 loss is associated with increased JNK activation upon suppression of oncogenic signaling by trametinib or the trametinib + AMG 176 combination.

To confirm these results, we examined JNK Thr183/Tyr185 phosphorylation in H2030 and H358 isogenic pairs. Combined sotorasib or trametinib + AMG 176 treatment led to a rapid time-dependent increase in JNK phosphorylation in H2030 EV cells (Fig. 2C, S5A) and JNK nuclear translocation (Fig. S5B). JNK activation could be suppressed by knockdown of MKK7, which phosphorylates and activates JNK (Fig. S5C). JNK activation was observed as rapidly as 2 hours after drug treatment and preceded apoptotic cell death (Fig. S5D), consistent with a proximal role for JNK activation in the apoptotic response. Re-expression of LKB1 suppressed JNK phosphorylation in H2030 cells, and conversely, deletion of LKB1 in H358 cells led to increased phospho-JNK after drug treatment (Fig. 2C, S5A). We extended these findings by comparing the induction of phospho-JNK across a larger cohort of *KRAS*-mutant NSCLC cells treated with trametinib + AMG 176. Despite an expected degree of heterogeneity between cell lines, LKB1-deficient cell lines overall exhibited greater induction of JNK phosphorylation compared to LKB1 wild-type cell lines with wild-type LKB1, with a significant correlation between pJNK induction and combination sensitivity (Fig. S5E). Interestingly, the H1792 cell line, which exhibited the greatest drug sensitivity amongst LKB1 wild-type cells (Fig. 1B), displayed robust induction of pJNK (Fig. S5F). Corroborating the results in H2030 cells, re-expression of LKB1 in H23 cells blunted the induction of phospho-JNK in response to trametinib + AMG 176 (Fig. S5G).

These data suggest that LKB1 suppresses JNK-dependent stress signaling that occurs upon inhibition of oncogenic signaling. As JNKs modulate cell proliferation, differentiation and survival in response a number of different environmental and cellular stressors[36], we examined whether hyperactivation of JNK signaling in LKB1-deficient cells is specific to MAPK inhibition or reflects a more general role for regulation of JNK by LKB1. Upon exposure of H2030 EV or LKB1 cells to UV light, a well-established inducer of JNK signaling[37,38], we observed an increase in phospho-JNK in H2030 EV cells that peaked within 60 minutes (Fig. S5H). Re-expression of LKB1 reduced UV-induced phospho-JNK in H2030 LKB1 cells, indicating that LKB1 may play a general role in suppressing JNK stress signaling in response to a variety of stimuli. To determine whether JNK activation underlies the increased sensitivity of LKB1-deficient *KRAS*-mutant cancer cells to combined MAPK + MCL-1 inhibition, we used siRNA to simultaneously knock down both JNK1 and 2 isoforms (Fig. S5I) and assessed the response to combined

sotorasib or trametinib + AMG 176. While JNK1/2 knockdown had little effect on sensitivity to trametinib alone, JNK1/2 depleted cells exhibited decreased sensitivity and apoptotic response to both drug combinations, phenocopying the effect of LKB1 re-expression (Fig. 2D-E, S5J-K). Collectively, these results suggest that hyper-activation of JNK signaling in the absence of LKB1 increases the MCL-1 dependence of LKB1-deficient *KRAS*-mutant NSCLC cells and sensitizes them to combined $KRAS^{G12C}$ or MEK + MCL-1 inhibition.

LKB1 exerts its effects via phosphorylation and activation of multiple members of the AMP-activated protein kinase (AMPK) family. For instance, LKB1 plays a central role in energy homeostasis by sensing increased intracellular AMP/ATP ratio and phosphorylating AMPK, which in turn suppresses energy consumption by inhibiting mTOR and stimulating autophagy[39]. Recently, the AMPK-related SIK kinases have been shown to play a major role in mediating the suppressive effects of LKB1 on tumorigenesis and metastatic potential in models of *KRAS*-mutant NSCLC[14,15]. However, a role for LKB1 in regulating apoptotic priming is largely undefined. To identify the LKB1 substrate kinase(s) that mediate the suppressive effect of LKB1 on drug-induced JNK activation and MCL-1 dependency, we simultaneously silenced the expression of multiple members within each AMPK-related kinase family that are expressed in NSCLC[15] (Fig. 2F, S6A-D). Silencing NUAK1+2 was sufficient to restore the sensitivity of H2030 LKB1 cells to combined sotorasib or trametinib + AMG 176 to a similar level as LKB1-deficient H2030 cells (Fig. 2G, S6E). In contrast, silencing SIKs, AMPKs or MARKs in the context of LKB1 re-expression did not restore drug sensitivity (Fig. 2G, S6F). The difference in drug sensitivity between LKB1-deficient and LKB1-restored cells was similar when cells were cultured in high or low/absent glucose conditions (Fig. S6G), consistent with a nutrient-independent mechanism. Knockdown of NUAK1/2 restored drug-induced JNK phosphorylation in H2030 cells expressing LKB1 to a similar level as H2030 control cells (Fig. 2H), and increased the apoptotic response of LKB1-expressing cells to trametinib + AMG 176 (Fig. S6H).

NUAKs regulate cell polarity[40], ploidy[41] and adhesion[42] through phosphorylation of the myosin phosphatase targeting-1 (MYPT1)-protein phosphatase-1beta (PP1B) complex. NUAK1 directly binds to and activates the PP1B phosphatase by displacing the self-inhibitory protein I-2[42]. We hypothesized that PP1B activation downstream of LKB1-NUAK1 could lead to dephosphorylation of JNK. Knockdown of PP1B expression dramatically increased pJNK in LKB1-restored H2030 cells (Fig. 2I) and increased sensitivity to MAPK + MCL-1 inhibition (Fig 2J, Fig. S6I), suggesting that PP1B de-phosphorylates JNK and reduces MCL-1 dependence downstream of LKB1. To demonstrate whether NUAK1 directly interacts with PP1B in LKB1-expressing *KRAS*-mutant NSCLC cells, we expressed HA-tagged NUAK1 in H2030 EV and LKB1 cells. Co-immunoprecipitation of PP1B revealed increased binding of NUAK to PP1B in H2030 LKB1 cells (Fig 2K, compare lanes 1 and 3) that was disrupted by mutation of the NUAK GILK domain (GKKK) that has been previously demonstrated to mediate the NUAK-PP1B interaction[42] (Fig. 2K, compare lanes 3 and 5). Conversely, binding of the I2 protein to PP1B was diminished in H2030 LKB1 cells and increased in the presence of the NUAK GKKK mutant, consistent with LKB1-dependent competition between NUAK and I2 for binding PP1B. Collectively, these results indicate that loss of LKB1-NUAK1/2 signaling leads to increased JNK signaling as a consequence of decreased PP1B phosphatase activity, resulting in increased sensitivity to combined MAPK + MCL-1 inhibition.

Inhibition of MEK/ERK signaling leads to BIM accumulation and increases apoptotic priming in oncogene-driven cancers treated with various targeted therapies, driving cells into an MCL-1 and/or BCL-XL dependent state[43,44]. To confirm that LKB1 modulates apoptotic priming, we performed BH3

profiling[45,46,47] on isogenic LKB1-deficient or WT cell lines before and after treatment with trametinib (Fig. S7A). As expected, trametinib treatment increased overall apoptotic priming (Fig. S7B). Trametinib induced a greater increase in MCL-1 specific priming (expressed as "Δ priming") in LKB1-deficient compared to LKB1 wild-type cells, and which was consistently reduced upon re-expression of LKB1 (Fig. S7C-D). Conversely, deletion of LKB1 in H358 cells increased trametinib-induced MCL-1 dependency. In a subset of cell lines, we also observed changes in BCL-XL dependency, however this was not a consistent effect (Fig. S7E). To investigate the basis for increased MCL-1 dependent priming in LKB1-deficient cells, we examined MCL-1 protein expression levels, as this is highly dependent on cap-dependent translational regulated by mTOR[48] (which is regulated by AMPK). Consistent with an AMPK-independent effect of LKB1, MCL-1 and BCL-XL protein expression was similar in LKB1-deficient and wild-type *KRAS*-mutant NSCLC cell lines (Fig. S7F-G) or isogenic cell line pairs (for example, see Fig. S8B). Next, we examined interactions between BIM and MCL-1 or BCL-XL. Co-immunoprecipitation (Co-IP) experiments revealed increased BIM bound to MCL-1 and BCL-XL after trametinib treatment (Fig. S8A-B), consistent with prior studies[28]. LKB1-deficient cells treated with trametinib had a greater amount of BIM bound to MCL-1, and less BIM bound to BCL-XL, compared to LKB1 wild-type cell lines (Fig. S8A-C). Restoration of LKB1 in deficient cell lines reduced the amount of BIM bound to MCL-1 after trametinib treatment, and knocking out LKB1 in wild-type cells increased the amount of BIM bound to MCL-1 (Fig. 3A, S8C-G). Notably, except for one cell line (A427), the impact of LKB1 re-expression/knock-down on baseline BIM:MCL-1 binding was less prominent in the absence of drug treatment. These results indicate that loss of LKB1 promotes the formation of BIM:MCL-1 complexes, especially in the context of suppression of oncogenic MAPK signaling, functionally inducing an MCL-1 dependent state and priming AMG 176 sensitivity.

MCL-1 and BCL-XL can be phosphorylated at multiple residues by numerous kinases, including JNK and ERK, leading to context-specific and divergent effects on protein stability/degradation, BIM binding affinity and apoptosis[49,50,51-54]. MCL-1 phosphorylation at T163 decreased acutely upon trametinib treatment consistent with a loss of ERK phosphorylation[55] and then rebounded at later time points coinciding with activation of JNK (Fig. S9A). Restoration of LKB1 in LKB1-deficient cells reduced the rebound in MCL-1 phosphorylation, while deleting LKB1 in wild-type cells increased MCL-1 phosphorylation (Fig. S9A-B). A similar time and JNK-dependent pattern of phosphorylation of BCL-XL at S62 was observed in LKB1-deficient cells, which was suppressed by re-expression of LKB1. Upon treatment with the combination of trametinib + AMG 176, BCL-XL S62 was rapidly phosphorylated in LKB1-deficient but not LKB1-proficient isogenic cell line pairs (Fig. 3B). Silencing JNK1/2 expression reduced drug-induced phosphorylation of both MCL-1 and BCL-XL to a similar level as the corresponding LKB1-restored isogenic cell line (Fig. S9C, compare lanes 3, 4 and 7). To assess whether JNK-mediated phosphorylation of MCL-1 or BCL-XL impacts drug sensitivity, we expressed DOX-inducible MCL-1 or BCL-XL phosphorylation-site mutants in H2030 cells while simultaneously knocking down expression of endogenous MCL-1 or BCL-XL (Fig. 3C, S9D-G). While mutating MCL-1 phosphorylation sites to alanine had little effect on sensitivity to trametinib + AMG 176 (Fig. 3D, S9H), expression of the BCL-XL S62A mutant reduced sensitivity to both sotorasib or trametinib + AMG 176 in H2030 and other cell lines (Fig. 3E-F, S9K), phenocopying LKB1 re-expression and JNK1/2 knockdown. Conversely, the BCL-XL S62E phosphomimetic increased the sensitivity of H2030 LKB1 cells (Fig. 3G). These results suggest that the increased MCL-1 dependency of LKB1-deficient cells is mediated by BCL-XL phosphorylation.

Prior studies have demonstrated that sensitivity of cancer cells to MCL-1 inhibition is inversely related to BCL-XL expression level and the capacity for BCL-XL to neutralize pro-apoptotic BH3 proteins such as BIM[56,57]. Phosphorylation of BCL-XL S62 induces a conformational change in which a dysregulated domain folds into the BCL-XL BH3 binding groove to prevent BIM binding[54]. Therefore, we hypothesized that phosphorylation of BCL-XL S62 by JNK compromises the ability of BCL-XL to sequester BIM that is liberated from MCL-1 upon MCL-1 inhibition. To test this, we studied the dynamics of BIM:MCL-1 and BIM:BCL-XL interactions by first treating cells with trametinib to increase BIM bound to MCL-1, then treating with a short pulse of AMG 176 and assessing the ability for BCL-XL to sequester BIM released from MCL-1 (Fig. 4A). In LKB1-deficient H2030 cells, very little BIM was sequestered by BCL-XL upon treatment with AMG 176, compared to LKB1 wild-type SW1573 cells, which exhibited substantial sequestration of BIM by BCL-XL (Fig. 4B). Restoring LKB1 expression or silencing JNK1/2 in H2030 cells increased the amount of BIM sequestered by BCL-XL after addition of AMG 176 (Fig. 4C-D). In H2030 and MGH1112-1 EV cells, the BCL-XL S62A mutant exhibited increased BIM:BCL-XL binding, whereas in H2030 LKB1 cells, the phospho-mimetic S62E mutant decreased BIM:BCL-XL binding (Fig. 4E-F, S9L). Knock-down of NUAK1/2 expression in H2030 cells, which we showed restored drug-induced JNK phosphorylation (Fig. 2H), restored the drug-induced phosphorylation of BCL-XL S62 (Fig. 4G). Collectively, these results demonstrate that in the context of LKB1 loss, activation of JNK creates an MCL-1 dependent state by phosphorylating BCL-XL and decreasing its capacity to buffer the pro-apoptotic effects of BIM (Fig. 4H). While in some cases, especially those that may be highly primed and MCL-1 dependent at baseline, LKB1 loss may confer sensitivity to MCL-1 inhibition alone, MCL-1 dependency is enhanced by the increase in apoptotic priming upon suppression of oncogenic MAPK signaling.

To investigate the clinical relevance of our findings, we performed BH3 profiling on *KRAS*-mutant NSCLCs (solid metastatic lesions or tumor cells isolated from malignant pleural effusions of patients) after *ex vivo* exposure to sotorasib or trametinib (Fig. 5A). Both sotorasib and trametinib treatment led to an increase in MCL-1 dependent priming (MS1 peptide) in *STK11/LKB1*-mutant but not WT tumors, (Fig. 5B, S10A). Consistent with this effect, co-immunoprecipitation experiments performed on tumor cells isolated from a malignant pleural effusion obtained from the same patient revealed drug-induced increases in BIM bound to MCL1 (Fig. 5C). In contrast, we did not observe a significant difference in drug-induced BCL-XL dependent priming (HRK peptide) between *STK11*-mutant and WT tumors. To extend these findings, we performed BH3 profiling on *KRAS*-mutant (G12C and other) NSCLC patient-derived xenograft (PDX) models with or without co-occurring *STK11* loss after short-term treatment with trametinib. Similar to the patient tumors and *in vitro* cell line models, LKB1-deficient tumors exhibited increased MCL-1-dependent priming compared to WT tumors (Fig 5D, S10B). The addition of AMG 176 to sotorasib led to greater tumor response than sotorasib alone in LKB1-deficient PDX tumors with MCL-1-dependent priming but not LKB1-deficient PDX tumors (Fig. 5E, S11A-C). To investigate potential toxicity, we assessed a combination dosing regimen with intermittent AMG 176 administration (AMG 176 is administered as intermittent infusions in currently on-going clinical trials) that induced similar tumor regression (Fig. S11D). In humanized MCL-1 knock-in mice[58] the combination of sotorasib with AMG 176 was well tolerated with no overt signs of toxicity (Fig. S11E). Consistent with the expected effects of on-target MCL-1 inhibition[58], we observed decreased B cells and monocytes, however no additional effects were observed in combination with sotorasib compared with AMG 176 alone (Fig S13F). Thus, loss of the LKB1 tumor suppressor is associated with increased MCL-1 dependence upon treatment with sotorasib or trametinib in $KRAS^{G12C}$-mutant NSCLCs, creating an apoptotic vulnerability that can be exploited by concurrent inhibition of MCL-1.

Discussion

While the utility of targeting truncal oncogenic driver mutations in lung cancer is firmly established, most clinical targeted therapy strategies do not take into account co-occurring mutations. For *KRAS*-mutant lung cancers in particular, identifying vulnerabilities associated with recurring co-occurring mutations in tumor suppressor genes could enable the development of biomarker-driven combination therapies with enhanced activity in distinct subsets of patients. However, the development of the most KRAS inhibitor drug combinations currently in the clinic has been agnostic to co-occurring mutations. Our finding that LKB1 regulates the apoptotic dependency of *KRAS*-mutant lung cancers is unexpected, as genomic features associated with sensitivity to BH3 mimetics in oncogene-addicted solid tumors have been elusive[28,43,59]. Inactivating mutations or loss of *STK11*/LKB1, which define one of the major genomic sub-groups of *KRAS*-mutant lung cancers[4,16,60], are of particular interest because they are associated with decreased responsiveness to immune checkpoint blockade[9,61] and poor overall prognosis[62].

LKB1 is a master kinase that regulates diverse cellular processes via phosphorylation of multiple members of AMPK family kinases[39,63]. In particular, the role of LKB1 in regulating energy homeostasis via AMPK has been well defined. In settings of energy stress (high AMP:ATP ratio), AMPK limits anabolic processes by inhibiting mTORC1 through TSC2[64]. Interestingly, expression levels of MCL-1 are highly dependent upon mTOR-mediated cap-dependent translation, and inhibition of mTOR by small-molecule inhibitors has been shown to reduce MCL-1 expression and confer apoptotic sensitivity[27]. We also observed an association between PI3K inhibition, MCL-1 down-regulation and AMG 176 sensitivity in LKB1-deficient *KRAS*-mutant NSCLC cell lines. However, we did not observe any change in MCL-1 expression upon manipulation of LKB1, and silencing AMPK expression did not phenocopy the effect of LKB1 loss on MCL-1 inhibitor sensitivity. Additionally, we did not observe a change in intracellular ROS upon restoration or deletion of LKB1 in our isogenic models (data not shown), nor did altering NADP/NADPH ratio change the sensitivity to MCL-1 inhibition (data not shown), arguing against AMPK-driven changes in metabolism[65,5], autophagy[66], mitochondrial defects[67,68] or ROS[7,69,70,71]. Collectively, these results support an AMPK-independent mechanism by which LKB1 modulates JNK signaling and MCL-1 dependency.

Beyond its role regulating metabolism via AMPK, LKB1 loss promotes tumorigenesis by reprogramming epigenetic states, facilitating lineage plasticity and promoting metastasis[7,70,72-74]. Recent studies have revealed a central role for the AMPK-related SIK kinases in mediating the suppressive effects of LKB1 on tumorigenesis[14,15]. The role of other AMPK-related kinases in mediating the tumor suppressor effects of LKB1 are not well defined. NUAK kinases have been shown to regulate cellular polarity, adhesion and cell cycle in normal tissues[40,42,75] and to play a critical role in neurite formation[76]. Our results reveal that NUAKs can function as negative regulators of JNK signaling, through binding and activation of the JNK phosphatase PP1B. To our knowledge, the LKB1/NUAK1/PP1B axis represents a novel mechanism by which LKB1 can suppress JNK stress signaling and regulate apoptosis. JNK has been reported to modulate apoptotic signaling by phosphorylating multiple pro- and anti-apoptotic BCL-2 family members, including BIM[77-80], BAX[81-83], BCL-XL[52,53] and MCL-1[49,51,84,85]. The consequences of differential phosphorylation are complex and can impact both protein stability/turnover as well as protein-protein interactions, leading to both pro- and anti-apoptotic effects in a context-specific manner. We observed JNK-mediated phosphorylation of both MCL-1 and BCL-XL in response to KRAS and MEK inhibition, however elimination of JNK phosphorylation sites in BCL-XL but not MCL-1 phenocopied the decrease in MCL-1 dependence observed with JNK knockdown or LKB1 re-expression. Future studies will be

necessary to determine whether JNK phosphorylation of MCL-1 may confer apoptotic vulnerabilities in other therapeutic contexts. Interestingly, we observed that a subset of LKB1-deficient cell lines exhibited sensitivity to single agent MCL-1 inhibition in the absence of MAPK inhibition, indicative of a highly-primed MCL-1-dependent baseline state. Re-expression of LKB1 partially decreased sensitivity to MCL-1 inhibition, suggesting that the baseline suppression of JNK by LKB1/NUAK may impact apoptotic dependency in the absence of therapeutic stress in some cases, which is further amplified by the increased apoptotic priming that occurs in the setting of suppression of oncogenic MAPK signaling.

While our study focused on *KRAS*-mutant lung cancers treated with KRAS or MEK inhibitor targeted therapies, we also provide evidence that LKB1 suppresses JNK activation in response to UV radiation, suggesting a fundamental role for LKB1 in regulating JNK stress signaling in response to a variety of stimuli. From an evolutionary perspective, we speculate that the ability for LKB1 to suppress JNK signaling may be advantageous in normal tissues facing energy or redox stress by temporarily suppressing apoptosis until compensatory mechanisms (also regulated by LKB1) can be engaged. It is less clear whether modulation of JNK signaling contributes to the tumor suppressor functions of LKB1, or whether the ability to hyperactivate JNK signaling provides an advantage to cancer cells with loss of LKB1. It is notable that the differential JNK activation and increase in MCL-1 dependency conferred by LKB1 loss was maximally observed in the setting of MAPK inhibition, suggesting that the functional effects of this pathway may be unmasked in specific contexts in response to select perturbations.

In summary, we identify a novel mechanism by which LKB1-NUAK regulates JNK stress signaling and modulates apoptotic dependencies in *KRAS*-mutant NSCLCs. In response to KRAS or MEK inhibition, LKB1-deficient cells exhibit hyperactivation of JNK and increased reliance on MCL-1 to buffer the increase in BIM. While LKB1-deficiency does not confer increased sensitivity to $KRAS^{G12C}$ or MEK inhibitors used as single agents, cells become primed for apoptosis when treated with MCL-1 BH3 mimetics. These results suggest a potential biomarker-informed combination therapy approach based on mutations or genomic loss of *STK11*/LKB1.

Methods

Cell culture

Commercially available *KRAS*-mutant NSCLC cell lines were obtained from the Center for Molecular Therapeutics at the Massachusetts General Hospital (MGH) Cancer Center and STR validation was performed at the initiation of the project (Biosynthesis, Inc.). Cell lines were routinely tested for mycoplasma during experimental use. Cell lines were maintained in RPMI supplemented with 5% FBS except A427, SW1573, H2009, H1573, which were maintained in DMEM/F12 supplemented with 5% FBS. Patient-derived NSCLC cell lines were established in our laboratory from surgical resections, core-needle biopsies, or pleural effusion samples as previously described, with the exception of the MGH1070 cell line, which was derived from a primary mouse PDX model. All patients signed informed consent to participate in a Dana- Farber/Harvard Cancer Center Institutional Review Board–approved protocol, giving permission for research to be performed on their samples. Clinically observed *KRAS* mutations (determined by MGH SNaPshot NGS genotyping panel) were verified in established cell lines. Established patient-derived cell lines were maintained in RPMI + 10% FBS.

Cell viability assessment

Cell viability was assessed using the CellTiter-Glo assay (Promega). Cells were seeded into 96-well plates 24 hours prior to drug addition, and cell proliferation was determined 72 hours after addition of drug by incubating cells with CellTiter-Glo reagent (50 µL/well) for 30 minutes on a shaking platform at room temperature. Luminescence was quantified using a SpectraMax i3x plate reader (MolecularDevices).

PI/Annexin apoptosis assay

Cells were seeded in triplicate at low density 24 hours prior to drug addition. Seventy-two hours after adding drugs, floating (dead) and adherent cells (alive) were collected and stained with propidium iodide (PI) and Cy5-Annexin V (BD Biosciences) and analyzed by flow cytometry. The annexin-positive apoptotic cell fraction was quantified using FlowJo software.

Generation of engineered cell lines

EV and LKB1 cell lines: EV (pBabe) and LKB1 retro-viral vectors were gifts from Dr. Kwok-Kin Wong (NYU). EV and LKB1 virus were prepared by transfecting HEK293 cells with EV or LKB1, VSV-G (Addgene #8454), Gag-Pol (Addgene #14887) using Lipofectamine 3000 (ThermoFisher) and collecting viral particles in the supernatant. Stable cell lines were generated by infecting *KRAS*-mutant NSCLC lines with EV or LKB1 virus followed by puromycin selection.

LKB1 knock-out cell lines: sgRNAs targeting the *STK11* locus were designed using CHOP-CHOP and cloned into pSpCas9(BB)-2A-GFP (Addgene #48138). *KRAS*-mutant NSCLC cell lines were transiently transfected with the plasmids and sorted for single clone formation by FACs. After clonal expansion, 20 clones were selected and loss of LKB1 expression was assessed by western blot. Alternatively, LKB1 sgRNAs were cloned into lentiCRISPR v2 (Addgene #52961). Lentiviral particles were prepared by transfecting HEK293 cells with EV or sgLKB1, VSV-G (Addgene #8454) and Δ8.91 using Lipofectamine 3000 (ThermoFisher). Stable cell lines were generated by infecting *KRAS*-mutant NSCLC lines with lentiCRISPR v2 or sgLKB1 virus followed by blasticidin selection.

DOX-inducible MCL-1, BCL-XL cell lines: Full length wild-type or mutant MCL-1, BCL-XL coding sequences were synthesized (GenScript) and cloned into pInducer20 (gift from Lee Zou, MGH). Lentiviral particles were prepared by transfecting HEK293 cells with pInducer20 or pInducer20-MCL-1/ pInducer20-BCL-XL, VSV-G (Addgene #8454) and Δ8.91 using Lipofectamine 3000 (ThermoFisher).

Stable cell lines were generated by infecting *KRAS*-mutant NSCLC lines were infected with EV or pInducer20-MCL-1 or pInducer20-BCL-XL virus followed by selection with neomycin/G418.

Mouse xenograft studies

All animal studies were conducted through Institutional Animal Care and Use Committee–approved animal protocols in accordance with institutional guidelines. *KRAS-mutant* NSCLC PDX models were generated from surgical resections, core-needle biopsies, or pleural effusion samples by subcutaneous implantation into NSG mice (Jackson Labs). Subcutaneous tumors were serially passaged twice to fully establish each model. Clinically observed *KRAS* mutations were verified in each established model. For drug studies, PDX tumors were directly implanted subcutaneously into NSG or athymic nude (NE/Nu) mice and allowed to grow to 250 to 400 mm^3. For H2030 xenograft studies, cell line suspensions were prepared in 1:1 matrigel:PBS, and 5×10^6 cells were injected unilaterally into the subcutaneous space on the flanks of athymic nude (Nu/Nu) mice and allowed to grow to approximately 350 mm^3. Tumors were measured with electronic calipers, and the tumor volume was calculated according to the formula $V = 0.52 \times L \times W^2$. Mice with established tumors were randomized to drug treatment groups using covariate adaptive randomization to minimize differences in baseline tumor volumes. Trametinib was dissolved in 0.5% HPMC/0.2% Tween 80 (pH 8.0) and administered by oral gavage daily at 3 mg/kg, 6 days per week. Sotorasib was dissolved in 2% HPMC/0.1% Tween 80 (pH 7) and administered by oral gavage daily at 100 mg/kg, 6 days per week. AMG 176 was dissolved in 25% hydroxypropylbeta- cyclodextrin (pH8.0) and administered by oral gavage daily 50 mg/kg.

Quantitative RT-PCR analysis

RNA was extracted using the Qiagen RNeasy kit. cDNA was prepared with the Transcriptor High Fidelity cDNA Synthesis Kit (Roche) using oligo-dT primers. Quantitative PCR was performed with gene specific primers (Supplemental table 2) using SYBR™ Select Master Mix (Applied biosystem) on a Lightcycler 480 (Thermofisher). Relative gene expression was calculated by using the Δ ΔCT method by normalizing to *ACTB.*

Western Blot analysis

Cells were seeded in either 6-well or 6 cm plates and drug was added when cells reached 70% confluency. Cells were harvested by washing twice with PBS, lysing in lysis buffer [28] on ice, and spinning at 14,000 RPM at 4ºC for 10 minutes to remove insoluble cell debris. Lysate protein concentrations were determined by a Bicinchoninic Acid assay (Thermo Fisher). Gel electrophoresis was performed using NuPage 4-12% Bis-Tris Midi gels (Invitrogen) in NuPage MOPS SDS Running Buffer (Invitrogen) followed by transfer onto PVDF membranes (Thermo Fisher). Following transfer, membranes blocked with 5% milk (Lab Scientific bioKEMIX) in Tris Buffered Saline with Tween 20 (TBS-T) and then incubated with primary antibody (1:1000, 1%BSA in TBS-T) at 4ºC overnight. After washing in TBS-T), membranes were incubated with the appropriate secondary antibody (1:12500 in 2% skim milk in TBS-T) for 1 hour at room temperature. The following HRP-linked secondary antibodies were used: anti-rabbit IgG (CST7074) and anti-mouse IgG (CST7076). Membranes were removed from secondary antibodies and washed 3 times for 10 minutes each in TBS-T. Prior to imaging, membranes were incubated for 4 minutes SuperSignal West Femto Stable Peroxide & Luminol/Enhancer (Thermo Fisher) diluted 1:10 in 0.1 M tris-HCL pH 8.8 (Boston Bioproducts). Luminescence was imaged using a G:Box Chemi-XRQ system (Syngene). The following primary antibodies were used: pJNK T183/Y185 (CST4668), SAPK/JNK (CST9252), BIM (CST2933), pBCL-XL S62 (Invitrogen 44-428G), BCL-XL (CST2764), LKB1 (CST3050), pMCL-1 T163 (CST14765), pMCL-1 S159/T163 (CST4579), pMCL-1 S64 (CST13297),

MCL-1 (BD Pharmingen 559027), pMKK4 S257/T261 (CST9156), MKK4 (CST9152), pMEK7 S271 (Thermo Fisher PA5-114604), pMEK7 T275 (Thermo Fisher PA5-114605), MKK7 (CST4172), DUSP10/MKP5 (CST3483), HA Tag (CST3724), β-Tubulin (CST2146), GAPDH (CST5174).

Protein Immunoprecipitation

Cells were seeded in either 10 cm or 15 cm plates and drug was added when cells reached 70% confluency. Cells were harvested after the treatment period and lysates were prepared using Tris Lysis Buffer with Protease Inhibitor Cocktail (Meso Scale Diagnostics) on ice. After normalization of total protein concentrations, Pierce Protein A/G Magnetic Beads (Thermo Fisher) and either mouse anti-human MCL-1 (BD Pharmingen 559027) or mouse anti-human BCL-XL (EMD Millipore MAB3121) antibodies were added to lysate aliquots and incubated at 4°C overnight. A representative aliquot of the normalized whole cell lysate was saved for Western blot analysis. The immunoprecipitated fractions were separate using magnetic separation, washed three times with Tris Lysis Buffer on ice, proteins eluted by heating at 95°C for 10 min with Tris Lysis Buffer and LDS Sample Buffer 4X (Invitrogen). For western blots, the rabbit anti-human MCL-1 (CST4572) antibody was used; all other antibodies were identical to those used for western blotting. For immunoprecipitation of HA-tagged BCL-XL, the Pierce Magnetic HA-Tag IP/Co-IP Kit (Thermo Fisher) was used following the manufacturer's protocol (specifically, the procedure for (A.) Manual IP/Co-IP and (B.) Elution Protocol 2 for reducing gel analysis).

Immunofluorescence and image analysis

Cells were fixed with 10% neutral-buffered formalin and permeabilized by PBST (PBS + Triton X100). Cells were then incubated with pJNK T183/Y185 (CST4668) primary antibody (1:400) overnight at 4°C. Secondary antibody staining was performed at room temperature for 1 hour, followed by DAPI staining. Images were acquired using a Zeiss LSM 710 confocal microscope. Image analysis was performed using CellProfiler software (Broad Institute). Briefly, individual cells were identified by DAPI staining. pJNK staining inside the nuclei or outside the nuclei was segmented and quantified at the individual cell level.

siRNA-Mediated Gene Knockdown

siRNA transfection was performed using Lipofectamine RNAiMAX Transfection Reagent according to the manufacturer's protocol (Invitrogen, Cat# 13778075). In brief, cells were seeded in 6-well, 6 cm, or 10 cm plates and siRNA transfection was carried out when cells reached ~70% confluency. Prior to transfection, cells were placed in antibiotic-free media. 48 hours after transfection, cells were seeded for analysis of proliferation or immunoprecipitation or harvested for western blot. The following Invitrogen siRNA were used: NC (AM4611), MAPK8 (ID: s11152), MAPK9 (ID: s11159), NUAK1 (ID: s90), NUAK2 (ID: s37779), PRKAA1 (ID: s100), PRKAA2 (ID: s11056), PRKAB1 (ID: s11059), PRKAB2 (ID: s11062), SIK1 (ID: s45377), SIK2 (ID: s23355), SIK3 (ID: s23712), MARK1 (ID: s8511), MARK2 (ID: s4648), MARK3 (ID: s8514), MARK4 (ID: s33718), MAP2K4 (ID: s11182, s11183), MAP2K7 (ID: s11183, s11184), MCL-1 (ID: s8584, s8585), BCL2L1 (ID: s1920, s1921, s1922).

BH3 Profiling of Cell Lines

BH3 profiling was performed by quantifying cytochrome c release upon addition of exogeneous BH3 peptide as previously described [45]. Briefly, $2x10^6$ cells were isolated, centrifuged at 500xg for 5 minutes, then the cell pellet was resuspended in 100µL PBS with 1µL Zombie Green viability dye (Biolegend, cat# 423111). Cells were stained at room temperature out of light for 15 minutes, then 400µL FACS Stain Buffer (2% FBS in PBS) was added to the sample to quench Zombie dye. Cells were then centrifuged at 500xg for 5 minutes then subjected to BH3 Profiling as previously described with indicated peptides and

concentrations. After BH3 profiling, cells were permeabilized for intra-cellular staining with a saponin-based buffer (1% saponin, 10% BSA in PBS) and stained with an antibody for Cytochrome C AlexaFluor 647 (Biolegend, 612310) used at 1:2000 dilution and DAPI. Cells were left to stain overnight at 4°C and analyzed by flow cytometry (Attune NxT) the following day.

BH3 Profiling of Primary Patient Samples

Surgical resections were minced by scalpels to ~1mm^3. Minced explants were cultured in RPMI1640 + 10% FBS overnight in the absence or presence of drugs. Immediately prior to BH3 profiling, tissue was further dissociated by collagenase/dispase enzymatic dissociation for 30 minutes at 37°C. Samples were then strained through 100µM filter to isolate single cells. For each sample, 2x10^6 cells were isolated, centrifuged at 500xg for 5 minutes, then the cell pellet was resuspended in 100µL PBS with 1µL Zombie Green viability dye (Biolegend, cat# 423111). Cells were stained at room temperature out of light for 15 minutes, then 400µL FACS Stain Buffer (2% FBS in PBS) was added to the sample to quench Zombie dye. Cells were then centrifuged at 500xg for 5 minutes, then resuspended in 100µL FACS Stain Buffer. Cells were then stained with the following conjugated cell-surface marker antibodies at 1:50 dilutions: CD326 (EpCAM) PE (Biolegend, 324206) and CD45 BV786 (Biolegend, 304048). Cells were then centrifuged at 500xg for 5 minutes and subjected to BH3 Profiling as previously described[45] with indicated peptides (e.g., MS1 = MCL-1, HRK = BCL-XL) and concentrations. After BH3 profiling, cells were permeabilized for intra-cellular staining with a saponin-based buffer (1% saponin, 10% BSA in PBS) and stained with an antibody for Cytochrome C AlexaFluor 647 (Biolegend, 612310) used at 1:2000 dilution and DAPI. Cells were left to stain overnight at 4°C and analyzed by flow cytometry (Attune NxT) the following day. Cells of interest were identified by positive DAPI, negative Zombie, negative CD45, and positive EpCAM staining.

Phosphoproteomic Analysis

Frozen cell pellets were lysed, obtained proteins reduced with DTT and alkylated with iodoacetamide, precipitated following the MeOH/CHCl3 protocol, and digested with LysC and trypsin, followed by phophopeptide enrichment as previously described[33,86,87]. For each sample 2.5 mg of peptides were either subjected to phosphopeptide enrichment on TiO2 beads (GL Sciences, Japan) or 1 mg of peptides were enriched via on Fe-NTA beads (Cube Biotech, Germany). Phosphopeptides were labeled with TMT10plex or TMTpro reagents (Thermo Fisher Scientific), pooled, and were fractionated into 24 fractions using basic pH reversed phase chromatography essentially as described previously[88]. Those were dried, re-suspended in 5% ACN/5% formic acid, and analyzed in 3-hour runs via LC-M2/MS3 on an Orbitrap FusionLumos mass spectrometer using the Simultaneous Precursor Selection (SPS) supported MS3 method[89,90] essentially as described previously[91]. Two MS2 spectra were acquired for each peptide using CID and HCD fragmentation as described earlier[92] and the gained MS2 spectra were assigned using a SEQUEST or COMET-based in-house built proteomics analysis platform[93] allowing phosphorylation of serine, threonine, and tyrosine residues as a variable modification. The Ascore algorithm was used to evaluate the correct assignment of phosphorylation within the peptide sequence[94]. Based on the target-decoy database search strategy[95] and employing linear discriminant analysis and posterior error histogram sorting, peptide and protein assignments were filtered to false discovery rate (FDR) of < 1%[93]. Peptides with sequences that were contained in more than one protein sequence from the UniProt database (2014) were assigned to the protein with most matching peptides[93]. Only MS3 with an average signal-to-noise value of larger than 40 per reporter ion as well as with an isolation specificity[90] of larger than 0.75 were considered for quantification. A two-step normalization of the protein TMT-intensities was performed by

first normalizing the protein intensities over all acquired TMT channels for each protein based on the median average protein intensity calculated for all proteins. To correct for slight mixing errors of the peptide mixture from each sample a median of the normalized intensities was calculated from all protein intensities in each TMT channel and the protein intensities were normalized to the median value of these median intensities.

Proteomic Analysis

50 µg of the of the resulting peptides after tryptic digest as described above were subsequently labeled using TMT-10plex reagents (Thermo Scientific) according to manufacturer's instructions. Labeled samples got combined and fractionated using a basic reversed phase hplc[88]. The resulting fractions were analyzed in an 3h reversed phase LC-MS2/MS3 run on an Orbitrap FusionLumos. MS3 isolation for quantification used Simultaneous Precursor Selection (SPS) as previously described[89-91]. Proteins were identified based on MS2 spectra using the sequest algorithm searching against a human data base (uniprot 2014)[96] using an in house-built platform[93]. Search strategy included a target-decoy database-based search in order to filter against a false-discovery rate (FDR) of protein identifications of less than 1%[95]. For quantification only MS3 with an average signal-to-noise value of larger than 40 per reporter ion as well as with an isolation specificity[90] of larger than 0.75 were considered and a two-step normalization as described above was performed.

Phospho-proteomic Signature Analysis

Phospho-signature analysis was performed using PTM-Signature Enrichment Analysis (PMT-SEA), a modified version of ssGSEA2.0 (https://github.com/broadinstitute/ssGSEA2.0). Briefly, relative log-fold increases/decreases were calculated by comparing the levels of phospho-peptides in each group. Relative log-fold increases/decreases were imported into the PMT-SEA package and compared against the PTM signatures database (PTMsigDB). Significant signatures were exported, ranked and compared between groups (for example LKB1-positive versus LKB1-negative isogenic pair).

Synergy analysis

Synergy analysis was performed using Biochemically Intuitive Generalized Loewe (BIGL)[97]. In short, NSCLC cell lines were treated with a matrix of increasing dose of Trametinib/Sotorasib with AMG 176 for 72 hours and cell viability was assessed by cell titer glow. Synergy analysis is divided into three parts: 1. Marginal curve was determined for each compound by using non-linear least squares estimation procedure. 2. Compute expected effect for "General Loewe model" from previously computed marginal curve. 3. Compare the expected response with observed viability by maxR statistical test, which evaluates whether the null model locally fits the observed data.

Statistical analysis

Significant testing for all experiments were performed by student t test, One-Way or Two-Way ANOVA. Specifically, Two-Way ANOVA were used for multiple comparisons of different groups of data corrected against Tukey hypothesis with 95% confidence interval.

Data availability

All phophoproteomic data (normalized intensity) can be downloaded from Harvard Dataverse using identifier https://doi.org/10.7910/DVN/OLVIT7. All other data supporting the findings of this study are available from the corresponding author on reasonable request.

Acknowledgements

We thank the patients and their families who provided tumor tissue for analysis and generation of patient-derived models. We thank members of the Hata lab and MGH Thoracic Oncology Group for helpful discussion and support. We thank Dr. Kwok-Kin Wong for providing the pBABE-EV and pBABE-LKB1 plasmids. This study was funded by support from the NIH F32 CA250231 (C.L.), Mark Foundation for Cancer Research (The EXTOL Project) (A.N.H.), Stand Up To Cancer–American Cancer Society Lung Cancer Dream Team Translational Research Grant (SU2C-AACR-DT17-15) (A.N.H.), the Ludwig Center at Harvard (A.N.H.), a research grant provided by Amgen, Inc. (A.N.H.), and by Be a Piece of the Solution Research Fund at MGH. Stand Up To Cancer (SU2C) is a division of the Entertainment Industry Foundation. Research grants are administered by the American Association for Cancer Research, the Scientific Partner of SU2C.

Author Contributions

C.L, M.U.S., Y.S., C.F., J.O., J.K., S.E..C, A.O., M.W. performed the experiments. R.H., J.L. contributed human samples and/or data. S.E.C., A.O., M.W. developed patient-derived cell lines and PDX models. C.L.**,** R.M. and A.N.H. performed data analysis and interpretation. S.C., A.Y.S., K.R., J.R.L., P.E.H. provided KRAS and MCL-1 inhibitors used in this study. C.L., J.O., C.N., K.S., W.H., P.E.H., A.N.H. were involved with study design. C.L. and A.N.H. wrote the manuscript. All authors discussed the results and commented on the manuscript.

Competing Interests Statement

A.N.H. has received research support from Amgen, Blueprint Medicines, BridgeBio, Bristol-Myers Squibb, C4 Therapeutics, Eli Lilly, Novartis, Nuvalent, Pfizer, Roche/Genentech and Scorpion Therapeutics; has served as a compensated consultant for Amgen, Engine Biosciences, Nuvalent, Oncovalent, Pfizer TigaTx, and Tolremo Therapeutics. RSH has served as a compensated consultant for Abbvie, Astrazeneca, Claim Therapeutics, Daichii Sankyo, EMD Serono, Lilly, Merck, Novartis, Regeneron, Sanofi. Research funding to institution, not to self: Abbvie, Agios, Corvus, Erasca, Genentech, Lilly, Mirati, Mythic, Novartis, Turning Point. J.J.L. reports consulting fees from Genentech, C4 Therapeutics, Blueprint Medicines, Nuvalent, Bayer, Elevation Oncology, Novartis, Mirati Therapeutics, and Turning Point Therapeutics; institutional research funding from Hengrui Therapeutics, Turning Point Therapeutics, Neon Therapeutics, Relay Therapeutics, Bayer, Elevation Oncology, Roche, Linnaeus Therapeutics, Nuvalent, and Novartis; and CME funding from OncLive, MedStar Health, and Northwell Health. C.S.N. owns equity (stock) in Opko Therapeutics and has received royalty income from ThermoFisher (previously Life Sciences). S.C., A.Y.S., K.R., R.L., B.B., J.R.L., P.E.H are employees of and have ownership (including stock, patents, etc.) interest in Amgen. The remaining authors declare no competing interests.

References:

1 Skoulidis, F. *et al.* STK11/LKB1 Mutations and PD-1 Inhibitor Resistance in KRAS-Mutant Lung Adenocarcinoma. *Cancer Discov* **8**, 822-835 (2018). https://doi.org:10.1158/2159-8290.CD-18-0099

2 Canale, M. *et al.* Impact of TP53 Mutations on Outcome in EGFR-Mutated Patients Treated with First-Line Tyrosine Kinase Inhibitors. *Clin Cancer Res* **23**, 2195-2202 (2017). https://doi.org:10.1158/1078-0432.CCR-16-0966

3 Vokes, N. I. *et al.* Concurrent TP53 Mutations Facilitate Resistance Evolution in EGFR-Mutant Lung Adenocarcinoma. *Journal of thoracic oncology : official publication of the International Association for the Study of Lung Cancer* **17**, 779-792 (2022). https://doi.org:10.1016/j.jtho.2022.02.011

4 Skoulidis, F. *et al.* Co-occurring genomic alterations define major subsets of KRAS-mutant lung adenocarcinoma with distinct biology, immune profiles, and therapeutic vulnerabilities. *Cancer Discov* **5**, 860-877 (2015). https://doi.org:10.1158/2159-8290.CD-14-1236

5 Jeon, S. M., Chandel, N. S. & Hay, N. AMPK regulates NADPH homeostasis to promote tumour cell survival during energy stress. *Nature* **485**, 661-665 (2012). https://doi.org:10.1038/nature11066

6 Nakada, D., Saunders, T. L. & Morrison, S. J. Lkb1 regulates cell cycle and energy metabolism in haematopoietic stem cells. *Nature* **468**, 653-658 (2010). https://doi.org:10.1038/nature09571

7 Ji, H. *et al.* LKB1 modulates lung cancer differentiation and metastasis. *Nature* **448**, 807-810 (2007). https://doi.org:nature06030 10.1038/nature06030

8 Liu, W. *et al.* LKB1/STK11 inactivation leads to expansion of a prometastatic tumor subpopulation in melanoma. *Cancer Cell* **21**, 751-764 (2012). https://doi.org:10.1016/j.ccr.2012.03.048

9 Skoulidis, F. *et al.* STK11/LKB1 Mutations and PD-1 Inhibitor Resistance in KRAS-Mutant Lung Adenocarcinoma. *Cancer Discov* (2018). https://doi.org:10.1158/2159-8290.CD-18-0099

10 Kitajima, S. *et al.* Suppression of STING Associated with LKB1 Loss in KRAS-Driven Lung Cancer. *Cancer Discov* **9**, 34-45 (2019). https://doi.org:10.1158/2159-8290.CD-18-0689

11 Shaw, R. J. *et al.* The tumor suppressor LKB1 kinase directly activates AMP-activated kinase and regulates apoptosis in response to energy stress. *Proc Natl Acad Sci U S A* **101**, 3329-3335 (2004). https://doi.org:10.1073/pnas.0308061100

12 Shaw, R. J. *et al.* The LKB1 tumor suppressor negatively regulates mTOR signaling. *Cancer Cell* **6**, 91-99 (2004). https://doi.org:10.1016/j.ccr.2004.06.007

13 Svensson, R. U. *et al.* Inhibition of acetyl-CoA carboxylase suppresses fatty acid synthesis and tumor growth of non-small-cell lung cancer in preclinical models. *Nat Med* **22**, 1108-1119 (2016). https://doi.org:10.1038/nm.4181

14 Hollstein, P. E. *et al.* The AMPK-Related Kinases SIK1 and SIK3 Mediate Key Tumor-Suppressive Effects of LKB1 in NSCLC. *Cancer Discov* **9**, 1606-1627 (2019). https://doi.org:10.1158/2159-8290.CD-18-1261

15 Murray, C. W. *et al.* An LKB1-SIK Axis Suppresses Lung Tumor Growth and Controls Differentiation. *Cancer Discov* **9**, 1590-1605 (2019). https://doi.org:10.1158/2159-8290.CD-18-1237

16 Cancer Genome Atlas Research, N. Comprehensive molecular profiling of lung adenocarcinoma. *Nature* **511**, 543-550 (2014). https://doi.org:10.1038/nature13385

17 Canon, J. *et al.* The clinical KRAS(G12C) inhibitor AMG 510 drives anti-tumour immunity. *Nature* **575**, 217-223 (2019). https://doi.org:10.1038/s41586-019-1694-1

18 Janne, P. A. *et al.* Adagrasib in Non-Small-Cell Lung Cancer Harboring a KRAS(G12C) Mutation. *N Engl J Med* **387**, 120-131 (2022). https://doi.org:10.1056/NEJMoa2204619

19 Skoulidis, F. *et al.* Sotorasib for Lung Cancers with KRAS p.G12C Mutation. *N Engl J Med* **384**, 2371-2381 (2021). https://doi.org:10.1056/NEJMoa2103695

20 Ryan, M. B. *et al.* Vertical Pathway Inhibition Overcomes Adaptive Feedback Resistance to KRAS(G12C) Inhibition. *Clin Cancer Res* **26**, 1633-1643 (2020). https://doi.org:10.1158/1078-0432.CCR-19-3523

21 Xue, J. Y. *et al.* Rapid non-uniform adaptation to conformation-specific KRAS(G12C) inhibition. *Nature* **577**, 421-425 (2020). https://doi.org:10.1038/s41586-019-1884-x

22 Misale, S. *et al.* KRAS G12C NSCLC Models Are Sensitive to Direct Targeting of KRAS in Combination with PI3K Inhibition. *Clin Cancer Res* **25**, 796-807 (2019). https://doi.org:10.1158/1078-0432.CCR-18-0368

23 Lou, K. *et al.* KRAS(G12C) inhibition produces a driver-limited state revealing collateral dependencies. *Sci Signal* **12** (2019). https://doi.org:10.1126/scisignal.aaw9450

24 Janes, M. R. *et al.* Targeting KRAS Mutant Cancers with a Covalent G12C-Specific Inhibitor. *Cell* **172**, 578-589 e517 (2018). https://doi.org:10.1016/j.cell.2018.01.006

25 Hallin, J. *et al.* The KRASG12C Inhibitor MRTX849 Provides Insight toward Therapeutic Susceptibility of KRAS-Mutant Cancers in Mouse Models and Patients. *Cancer Discovery* **10**, 54-71 (2020). https://doi.org:10.1158/2159-8290.cd-19-1167

26 Faber, A. C. *et al.* Differential induction of apoptosis in HER2 and EGFR addicted cancers following PI3K inhibition. *Proc Natl Acad Sci U S A* **106**, 19503-19508 (2009). https://doi.org:10.1073/pnas.0905056106

27 Faber, A. C. *et al.* mTOR inhibition specifically sensitizes colorectal cancers with KRAS or BRAF mutations to BCL-2/BCL-XL inhibition by suppressing MCL-1. *Cancer Discov* **4**, 42-52 (2014). https://doi.org:10.1158/2159-8290.CD-13-0315

28 Nangia, V. *et al.* Exploiting MCL1 Dependency with Combination MEK + MCL1 Inhibitors Leads to Induction of Apoptosis and Tumor Regression in KRAS-Mutant Non-Small Cell Lung Cancer. *Cancer Discov* (2018). https://doi.org:10.1158/2159-8290.CD-18-0277

29 Inoki, K., Zhu, T. & Guan, K. L. TSC2 mediates cellular energy response to control cell growth and survival. *Cell* **115**, 577-590 (2003). https://doi.org:10.1016/s0092-8674(03)00929-2

30 Baas, A. F. *et al.* Complete polarization of single intestinal epithelial cells upon activation of LKB1 by STRAD. *Cell* **116**, 457-466 (2004). https://doi.org:10.1016/s0092-8674(04)00114-x

31 Shelly, M., Cancedda, L., Heilshorn, S., Sumbre, G. & Poo, M. M. LKB1/STRAD promotes axon initiation during neuronal polarization. *Cell* **129**, 565-577 (2007). https://doi.org:10.1016/j.cell.2007.04.012

32 Barnes, A. P. *et al.* LKB1 and SAD kinases define a pathway required for the polarization of cortical neurons. *Cell* **129**, 549-563 (2007). https://doi.org:10.1016/j.cell.2007.03.025

33 Kreuzer, J., Edwards, A. & Haas, W. Multiplexed quantitative phosphoproteomics of cell line and tissue samples. *Methods Enzymol* **626**, 41-65 (2019). https://doi.org:10.1016/bs.mie.2019.07.027

34 Krug, K. *et al.* A Curated Resource for Phosphosite-specific Signature Analysis. *Mol Cell Proteomics* **18**, 576-593 (2019). https://doi.org:10.1074/mcp.TIR118.000943

35 Pumiglia, K. M. & Decker, S. J. Cell cycle arrest mediated by the MEK/mitogen-activated protein kinase pathway. *Proc Natl Acad Sci U S A* **94**, 448-452 (1997). https://doi.org:10.1073/pnas.94.2.448

36 Wagner, E. F. & Nebreda, A. R. Signal integration by JNK and p38 MAPK pathways in cancer development. *Nat Rev Cancer* **9**, 537-549 (2009). https://doi.org:10.1038/nrc2694

37 Derijard, B. *et al.* JNK1: a protein kinase stimulated by UV light and Ha-Ras that binds and phosphorylates the c-Jun activation domain. *Cell* **76**, 1025-1037 (1994). https://doi.org:10.1016/0092-8674(94)90380-8

38 Hibi, M., Lin, A., Smeal, T., Minden, A. & Karin, M. Identification of an oncoprotein- and UV-responsive protein kinase that binds and potentiates the c-Jun activation domain. *Genes Dev* **7**, 2135-2148 (1993). https://doi.org:10.1101/gad.7.11.2135

39 Shackelford, D. B. & Shaw, R. J. The LKB1-AMPK pathway: metabolism and growth control in tumour suppression. *Nat Rev Cancer* **9**, 563-575 (2009). https://doi.org:10.1038/nrc2676

40 Amin, N. *et al.* LKB1 regulates polarity remodeling and adherens junction formation in the Drosophila eye. *Proc Natl Acad Sci U S A* **106**, 8941-8946 (2009). https://doi.org:10.1073/pnas.0812469106

41 Humbert, N. *et al.* Regulation of ploidy and senescence by the AMPK-related kinase NUAK1. *EMBO J* **29**, 376-386 (2010). https://doi.org:10.1038/emboj.2009.342

42 Zagorska, A. *et al.* New roles for the LKB1-NUAK pathway in controlling myosin phosphatase complexes and cell adhesion. *Sci Signal* **3**, ra25 (2010). https://doi.org:10.1126/scisignal.2000616

43 Cragg, M. S., Harris, C., Strasser, A. & Scott, C. L. Unleashing the power of inhibitors of oncogenic kinases through BH3 mimetics. *Nat Rev Cancer* **9**, 321-326 (2009). https://doi.org:10.1038/nrc2615

44 Hata, A. N., Engelman, J. A. & Faber, A. C. The BCL2 Family: Key Mediators of the Apoptotic Response to Targeted Anticancer Therapeutics. *Cancer Discov* **5**, 475-487 (2015). https://doi.org:10.1158/2159-8290.CD-15-0011

45 Montero, J. *et al.* Drug-induced death signaling strategy rapidly predicts cancer response to chemotherapy. *Cell* **160**, 977-989 (2015). https://doi.org:10.1016/j.cell.2015.01.042

46 Ni Chonghaile, T. *et al.* Pretreatment mitochondrial priming correlates with clinical response to cytotoxic chemotherapy. *Science* **334**, 1129-1133 (2011). https://doi.org:10.1126/science.1206727

47 Fraser, C., Ryan, J. & Sarosiek, K. BH3 Profiling: A Functional Assay to Measure Apoptotic Priming and Dependencies. *Methods Mol Biol* **1877**, 61-76 (2019). https://doi.org:10.1007/978-1-4939-8861-7_4

48 Mills, J. R. *et al.* mTORC1 promotes survival through translational control of Mcl-1. *Proc Natl Acad Sci U S A* **105**, 10853-10858 (2008). https://doi.org:10.1073/pnas.0804821105

49 Morel, C., Carlson, S. M., White, F. M. & Davis, R. J. Mcl-1 integrates the opposing actions of signaling pathways that mediate survival and apoptosis. *Mol Cell Biol* **29**, 3845-3852 (2009). https://doi.org:10.1128/MCB.00279-09

50 Inoshita, S. *et al.* Phosphorylation and inactivation of myeloid cell leukemia 1 by JNK in response to oxidative stress. *J Biol Chem* **277**, 43730-43734 (2002). https://doi.org:10.1074/jbc.M207951200

51 Pan, R. *et al.* Synthetic Lethality of Combined Bcl-2 Inhibition and p53 Activation in AML: Mechanisms and Superior Antileukemic Efficacy. *Cancer Cell* **32**, 748-760 e746 (2017). https://doi.org:10.1016/j.ccell.2017.11.003

52 El Fajoui, Z. *et al.* Oxaliplatin sensitizes human colon cancer cells to TRAIL through JNK-dependent phosphorylation of Bcl-xL. *Gastroenterology* **141**, 663-673 (2011). https://doi.org:10.1053/j.gastro.2011.04.055

53 Kharbanda, S. *et al.* Translocation of SAPK/JNK to mitochondria and interaction with Bcl-x(L) in response to DNA damage. *J Biol Chem* **275**, 322-327 (2000). https://doi.org:10.1074/jbc.275.1.322

54 Follis, A. V. *et al.* Regulation of apoptosis by an intrinsically disordered region of Bcl-xL. *Nat Chem Biol* **14**, 458-465 (2018). https://doi.org:10.1038/s41589-018-0011-x

55 Domina, A. M., Vrana, J. A., Gregory, M. A., Hann, S. R. & Craig, R. W. MCL1 is phosphorylated in the PEST region and stabilized upon ERK activation in viable cells, and at additional sites with cytotoxic okadaic acid or taxol. *Oncogene* **23**, 5301-5315 (2004). https://doi.org:10.1038/sj.onc.1207692

56 Kotschy, A. *et al.* The MCL1 inhibitor S63845 is tolerable and effective in diverse cancer models. *Nature* **538**, 477-482 (2016). https://doi.org:10.1038/nature19830

57 Caenepeel, S. *et al.* AMG 176, a Selective MCL1 Inhibitor, Is Effective in Hematologic Cancer Models Alone and in Combination with Established Therapies. *Cancer Discov* (2018). https://doi.org:10.1158/2159-8290.CD-18-0387

58 Caenepeel, S. *et al.* AMG 176, a Selective MCL1 Inhibitor, Is Effective in Hematologic Cancer Models Alone and in Combination with Established Therapies. *Cancer Discov* **8**, 1582-1597 (2018). https://doi.org:10.1158/2159-8290.CD-18-0387

59 Corcoran, R. B. *et al.* Synthetic lethal interaction of combined BCL-XL and MEK inhibition promotes tumor regressions in KRAS mutant cancer models. *Cancer Cell* **23**, 121-128 (2013). https://doi.org:10.1016/j.ccr.2012.11.007

60 Jordan, E. J. *et al.* Prospective Comprehensive Molecular Characterization of Lung Adenocarcinomas for Efficient Patient Matching to Approved and Emerging Therapies. *Cancer Discov* **7**, 596-609 (2017). https://doi.org:10.1158/2159-8290.CD-16-1337

61 Ricciuti, B. *et al.* Diminished Efficacy of Programmed Death-(Ligand)1 Inhibition in STK11- and KEAP1-Mutant Lung Adenocarcinoma Is Affected by KRAS Mutation Status. *J Thorac Oncol* **17**, 399-410 (2022). https://doi.org:10.1016/j.jtho.2021.10.013

62 Rosellini, P. *et al.* Clinical impact of STK11 mutation in advanced-stage non-small cell lung cancer. *Eur J Cancer* **172**, 85-95 (2022). https://doi.org:10.1016/j.ejca.2022.05.026

63 Kullmann, L. & Krahn, M. P. Controlling the master-upstream regulation of the tumor suppressor LKB1. *Oncogene* **37**, 3045-3057 (2018). https://doi.org:10.1038/s41388-018-0145-z

64 Van Nostrand, J. L. *et al.* AMPK regulation of Raptor and TSC2 mediate metformin effects on transcriptional control of anabolism and inflammation. *Genes Dev* **34**, 1330-1344 (2020). https://doi.org:10.1101/gad.339895.120

65 Pooya, S. *et al.* The tumour suppressor LKB1 regulates myelination through mitochondrial metabolism. *Nat Commun* **5**, 4993 (2014). https://doi.org:10.1038/ncomms5993

66 Egan, D. F. *et al.* Phosphorylation of ULK1 (hATG1) by AMP-activated protein kinase connects energy sensing to mitophagy. *Science* **331**, 456-461 (2011). https://doi.org:10.1126/science.1196371

67 Gan, B. *et al.* Lkb1 regulates quiescence and metabolic homeostasis of haematopoietic stem cells. *Nature* **468**, 701-704 (2010). https://doi.org:10.1038/nature09595

68 Shackelford, D. B. *et al.* LKB1 inactivation dictates therapeutic response of non-small cell lung cancer to the metabolism drug phenformin. *Cancer Cell* **23**, 143-158 (2013). https://doi.org:10.1016/j.ccr.2012.12.008

69 Galan-Cobo, A. *et al.* LKB1 and KEAP1/NRF2 Pathways Cooperatively Promote Metabolic Reprogramming with Enhanced Glutamine Dependence in KRAS-Mutant Lung Adenocarcinoma. *Cancer Res* **79**, 3251-3267 (2019). https://doi.org:10.1158/0008-5472.CAN-18-3527

70 Li, F. *et al.* LKB1 Inactivation Elicits a Redox Imbalance to Modulate Non-small Cell Lung Cancer Plasticity and Therapeutic Response. *Cancer Cell* **27**, 698-711 (2015). https://doi.org:10.1016/j.ccell.2015.04.001

71 Hayes, J. D., Dinkova-Kostova, A. T. & Tew, K. D. Oxidative Stress in Cancer. *Cancer Cell* **38**, 167-197 (2020). https://doi.org:10.1016/j.ccell.2020.06.001

72 Zhang, H. *et al.* Lkb1 inactivation drives lung cancer lineage switching governed by Polycomb Repressive Complex 2. *Nat Commun* **8**, 14922 (2017). https://doi.org:10.1038/ncomms14922

73 Pierce, S. E. *et al.* LKB1 inactivation modulates chromatin accessibility to drive metastatic progression. *Nat Cell Biol* **23**, 915-924 (2021). https://doi.org:10.1038/s41556-021-00728-4

74 Murray, C. W. *et al.* LKB1 drives stasis and C/EBP-mediated reprogramming to an alveolar type II fate in lung cancer. *Nat Commun* **13**, 1090 (2022). https://doi.org:10.1038/s41467-022-28619-8

75 Banerjee, S., Zagorska, A., Deak, M., Campbell, D. G., Prescott, A. R. & Alessi, D. R. Interplay between Polo kinase, LKB1-activated NUAK1 kinase, PP1betaMYPT1 phosphatase complex and the SCFbetaTrCP E3 ubiquitin ligase. *Biochem J* **461**, 233-245 (2014). https://doi.org:10.1042/BJ20140408

76 Blazejewski, S. M., Bennison, S. A., Liu, X. & Toyo-Oka, K. High-throughput kinase inhibitor screening reveals roles for Aurora and Nuak kinases in neurite initiation and dendritic branching. *Sci Rep* **11**, 8156 (2021). https://doi.org:10.1038/s41598-021-87521-3

77 Lei, K. & Davis, R. J. JNK phosphorylation of Bim-related members of the Bcl2 family induces Bax-dependent apoptosis. *Proc Natl Acad Sci U S A* **100**, 2432-2437 (2003). https://doi.org:10.1073/pnas.0438011100

78 Hubner, A., Barrett, T., Flavell, R. A. & Davis, R. J. Multisite phosphorylation regulates Bim stability and apoptotic activity. *Mol Cell* **30**, 415-425 (2008). https://doi.org:10.1016/j.molcel.2008.03.025

79 Becker, E. B., Howell, J., Kodama, Y., Barker, P. A. & Bonni, A. Characterization of the c-Jun N-terminal kinase-BimEL signaling pathway in neuronal apoptosis. *J Neurosci* **24**, 8762-8770 (2004). https://doi.org:10.1523/JNEUROSCI.2953-04.2004

80 Corazza, N. *et al.* TRAIL receptor-mediated JNK activation and Bim phosphorylation critically regulate Fas-mediated liver damage and lethality. *J Clin Invest* **116**, 2493-2499 (2006). https://doi.org:10.1172/JCI27726

81 Tsuruta, F. *et al.* JNK promotes Bax translocation to mitochondria through phosphorylation of 14-3-3 proteins. *EMBO J* **23**, 1889-1899 (2004). https://doi.org:10.1038/sj.emboj.7600194

82 Park, G. B., Choi, Y., Kim, Y. S., Lee, H. K., Kim, D. & Hur, D. Y. ROS-mediated JNK/p38-MAPK activation regulates Bax translocation in Sorafenib-induced apoptosis of EBV-transformed B cells. *Int J Oncol* **44**, 977-985 (2014). https://doi.org:10.3892/ijo.2014.2252

83 Robitaille, K., Daviau, A., Lachance, G., Couture, J. P. & Blouin, R. Calphostin C-induced apoptosis is mediated by a tissue transglutaminase-dependent mechanism involving the DLK/JNK signaling pathway. *Cell Death Differ* **15**, 1522-1531 (2008). https://doi.org:10.1038/cdd.2008.77

84 Tong, J. *et al.* Mcl-1 Phosphorylation without Degradation Mediates Sensitivity to HDAC Inhibitors by Liberating BH3-Only Proteins. *Cancer Res* **78**, 4704-4715 (2018). https://doi.org:10.1158/0008-5472.CAN-18-0399

85 Mazumder, S., Choudhary, G. S., Al-Harbi, S. & Almasan, A. Mcl-1 Phosphorylation defines ABT-737 resistance that can be overcome by increased NOXA expression in leukemic B cells. *Cancer Res* **72**, 3069-3079 (2012). https://doi.org:10.1158/0008-5472.CAN-11-4106

86 Leutert, M., Rodriguez-Mias, R. A., Fukuda, N. K. & Villen, J. R2-P2 rapid-robotic phosphoproteomics enables multidimensional cell signaling studies. *Mol Syst Biol* **15**, e9021 (2019). https://doi.org:10.15252/msb.20199021

87 Liu, X. *et al.* Fe(3+)-NTA magnetic beads as an alternative to spin column-based phosphopeptide enrichment. *J Proteomics* **260**, 104561 (2022). https://doi.org:10.1016/j.jprot.2022.104561

88 Edwards, A. & Haas, W. Multiplexed Quantitative Proteomics for High-Throughput Comprehensive Proteome Comparisons of Human Cell Lines. *Methods Mol Biol* **1394**, 1-13 (2016). https://doi.org:10.1007/978-1-4939-3341-9_1

89 McAlister, G. C. *et al.* MultiNotch MS3 enables accurate, sensitive, and multiplexed detection of differential expression across cancer cell line proteomes. *Anal Chem* **86**, 7150-7158 (2014). https://doi.org:10.1021/ac502040v

90 Ting, L., Rad, R., Gygi, S. P. & Haas, W. MS3 eliminates ratio distortion in isobaric multiplexed quantitative proteomics. *Nat Methods* **8**, 937-940 (2011). https://doi.org:10.1038/nmeth.1714

91 Erickson, B. K., Jedrychowski, M. P., McAlister, G. C., Everley, R. A., Kunz, R. & Gygi, S. P. Evaluating multiplexed quantitative phosphopeptide analysis on a hybrid quadrupole mass filter/linear ion trap/orbitrap mass spectrometer. *Anal Chem* **87**, 1241-1249 (2015). https://doi.org:10.1021/ac503934f

92 Lyons, J. *et al.* Integrated in vivo multiomics analysis identifies p21-activated kinase signaling as a driver of colitis. *Sci Signal* **11** (2018). https://doi.org:10.1126/scisignal.aan3580

93 Huttlin, E. L. *et al.* A tissue-specific atlas of mouse protein phosphorylation and expression. *Cell* **143**, 1174-1189 (2010). https://doi.org:10.1016/j.cell.2010.12.001

94 Beausoleil, S. A., Villen, J., Gerber, S. A., Rush, J. & Gygi, S. P. A probability-based approach for high-throughput protein phosphorylation analysis and site localization. *Nat Biotechnol* **24**, 1285-1292 (2006). https://doi.org:10.1038/nbt1240

95 Elias, J. E. & Gygi, S. P. Target-decoy search strategy for increased confidence in large-scale protein identifications by mass spectrometry. *Nat Methods* **4**, 207-214 (2007). https://doi.org:10.1038/nmeth1019

96 Eng, J. K., McCormack, A. L. & Yates, J. R. An approach to correlate tandem mass spectral data of peptides with amino acid sequences in a protein database. *J Am Soc Mass Spectrom* **5**, 976-989 (1994). https://doi.org:10.1016/1044-0305(94)80016-2

97 Van der Borght, K. *et al.* BIGL: Biochemically Intuitive Generalized Loewe null model for prediction of the expected combined effect compatible with partial agonism and antagonism. *Sci Rep* **7**, 17935 (2017). https://doi.org:10.1038/s41598-017-18068-5

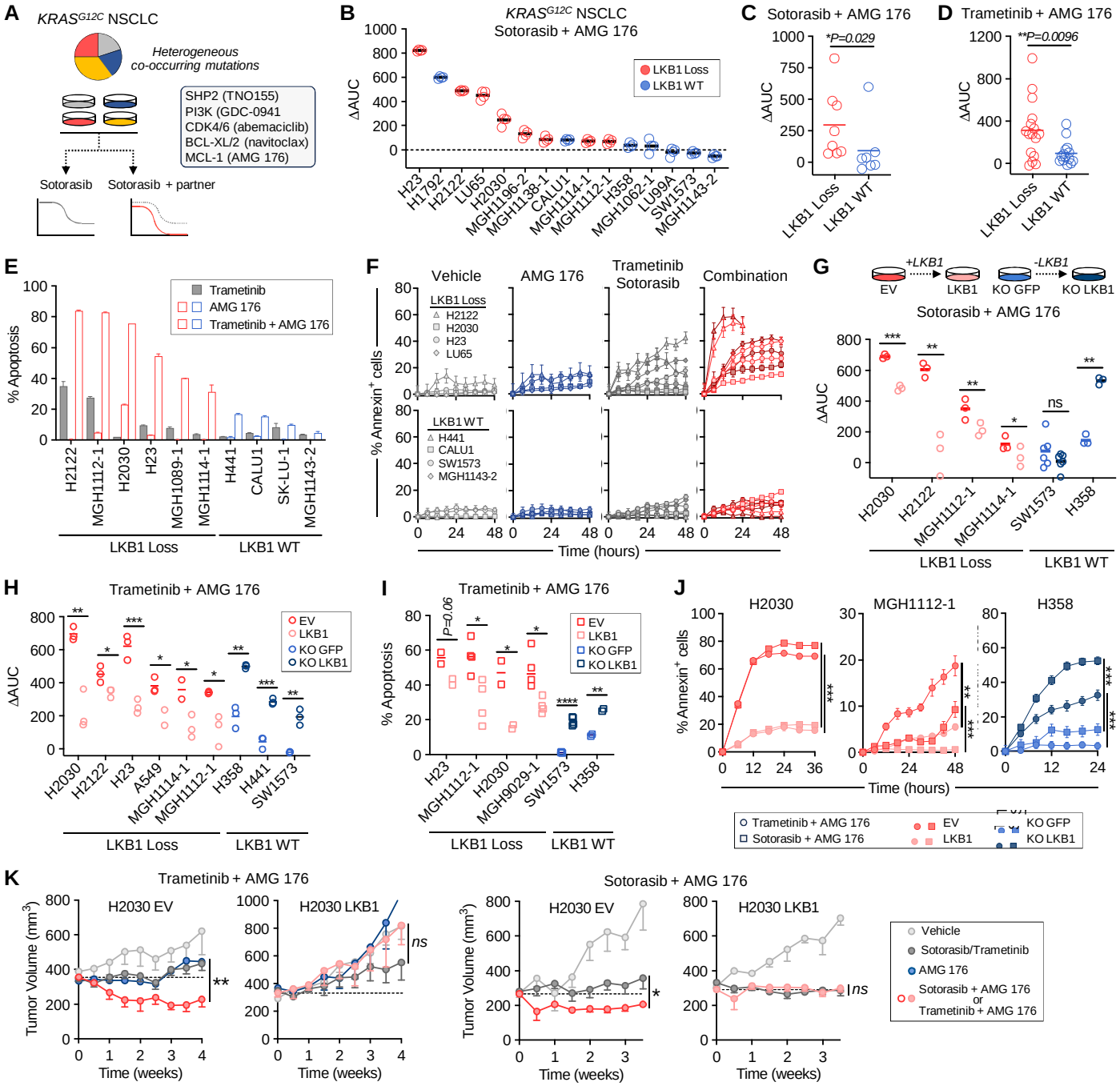

Figure 1. LKB1 loss confers sensitivity to combined MAPK + MCL-1 inhibition in *KRAS*-mutant NSCLC models. A. Schema for testing sotorasib drug combinations. **B.** Relative increased efficacy of sotorasib + AMG 176 combination compared to sotorasib alone (ΔAUC – see Fig. S1D for explanation) against *KRAS*^{G12C}-mutant NSCLC cell lines. Each dot represents an independent biological replicate (N=4). **C-D.** Comparison of ΔAUC between *KRAS*-mutant NSCLC cell lines stratified according to *LKB1* status (Mann Whitney t test). **E-F.** *KRAS*-mutant NSCLC cell lines were treated with 0.1 μM of trametinib, 1 μM of AMG 176 or the combination for up to 72 hours and apoptosis was assessed by annexin positivity by flow cytometry (E, data are mean and S.E.M. of 3 biological replicates) or live-cell imaging (F, data are mean and S.E.M. of 3 technical replicates). **G-H.** Comparison of relative ΔAUC for isogenic LKB1-proficient and deficient *KRAS*-mutant cell line pairs (EV - empty vector, LKB1 – LKB1 expression vector; KO GFP – GFP sgRNA, KO LKB1 – LKB1 sgRNA). Each dot represents an independent biological replicate (N=3-4). **I-J.** Apoptotic response of isogenic *KRAS*-mutant NSCLC cell lines after treatment with 0.1 μM trametinib or 1 μM sotorasib in combination with 1 μM of AMG 176 (annexin positivity assessed by flow cytometry (I, each dot represents an independent biological replicate, N=3) or live-cell imaging (J, data are mean and S.E.M. of 3 technical replicates). **K.** Subcutaneous xenograft tumors were established from H2030 EV and H2030 LKB1 cell lines and mice were treated with vehicle, sotorasib (30 mg/kg daily), trametinib (3 mg/kg daily), AMG 176 (50 mg/kg daily) or combination. Data shown are mean and S.E.M of N=5-6 mice per arm, statistical difference between single agent and combination arms was determined using mixed effects model (*p<0.05, **p<0.01).

Figure 1

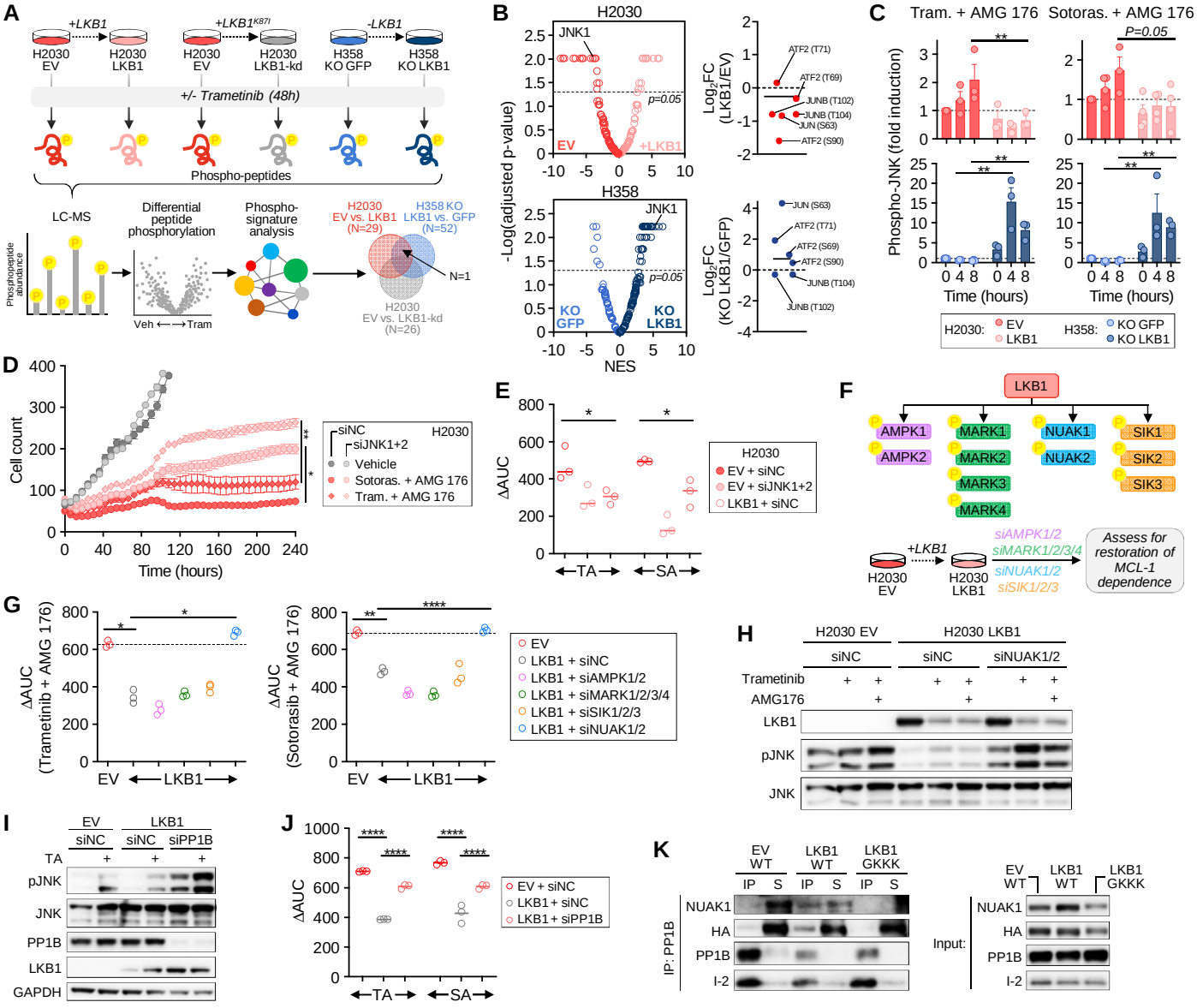

Figure 2. JNK activation in LKB1-deficient cells underlies dependency on MCL-1. A. Phosphoproteomic analysis of isogenic *KRAS*-mutant NSCLC cell lines treated with 0.1 μM of trametinib for 48 hours or 0.1 μM of trametinib + AMG 176 for 6 hours. **B.** Differential enrichment of phosphopeptide signatures in trametinib-treated isogenic cell line pairs. Phosphopeptide signatures and normalized enrichment scores (NES) were calculated using ssGSEA2.0/PTM-SEA. Right, individual phospho-sites of JNK1 downstream substrates are annotated. **C.** Change in JNK phosphorylation in response to MAPK + MCL-1 inhibition in isogenic H2030 and H358 cells (data are mean and S.E.M., each dot represents an independent biological replicate, N=3). **D.** Change in cell number of H2030 EV cells with siRNA knockdown of JNK1+2 or negative control (siNC) after treatment with 0.1 μM trametinib or 1 μM sotorasib in combination with 1 μM AMG 176 quantified by live-cell imaging. Data are mean and S.E.M. of 3 technical replicates. **E.** Knockdown of JNK1+2 gene expression decreases ΔAUC, phenocopying LKB1 re-expression. H2030 EV cells or H2030 LBK1 cells were transfected with siRNAs targeting JNK1 and 2 or negative control (siNC) and then treated with sotorasib (S) or trametinib (T) in the absence or presence of AMG 176 (A) and viability was determined after 3 days. Each dot represents an independent biological replicate (N=3). **F.** Schematic of siRNA knockdown of LKB1 effectors in H2030 LKB1 cells. **G.** Knockdown of NUAK1/2 restores sensitivity (ΔAUC) to combined sotorasib or trametinib + AMG 176. H2030 EV cells or H2030 LBK1 cells transfected with corresponding siRNAs were treated with sotorasib or trametinib in the absence or presence of AMG 176 (1 μM) and viability was determined after 3 days. Each dot represents an independent biological replicate (N=3). **H-I.** NUAK1/2 or PP1B knockdown restores phospho-JNK induction after trametinib or trametinib + AMG 176 in H2030 LKB1 cells to the level of H2030 control cells. Cells were transfected with the indicated siRNAs and then treated with trametinib (0.1 μM) for 48 hours or trametinib for 48 hours followed by AMG 176 for 4 hours. **J.** Knockdown of PP1B restores sensitivity (ΔAUC) to combined sotorasib or trametinib + AMG 176. Each dot represents an independent biological replicate (N=3). **K.** Restoration of LKB1 expression induces binding between PPIB and WT NUAK1, but not GKKK mutant. HA-tagged WT NUAK1 (WT) or GKKK NUAK were over-expressed in H2030 isogenic cells and the interaction of NUAK1 and PP1B was assessed by immuno-precipitation.

Figure 2

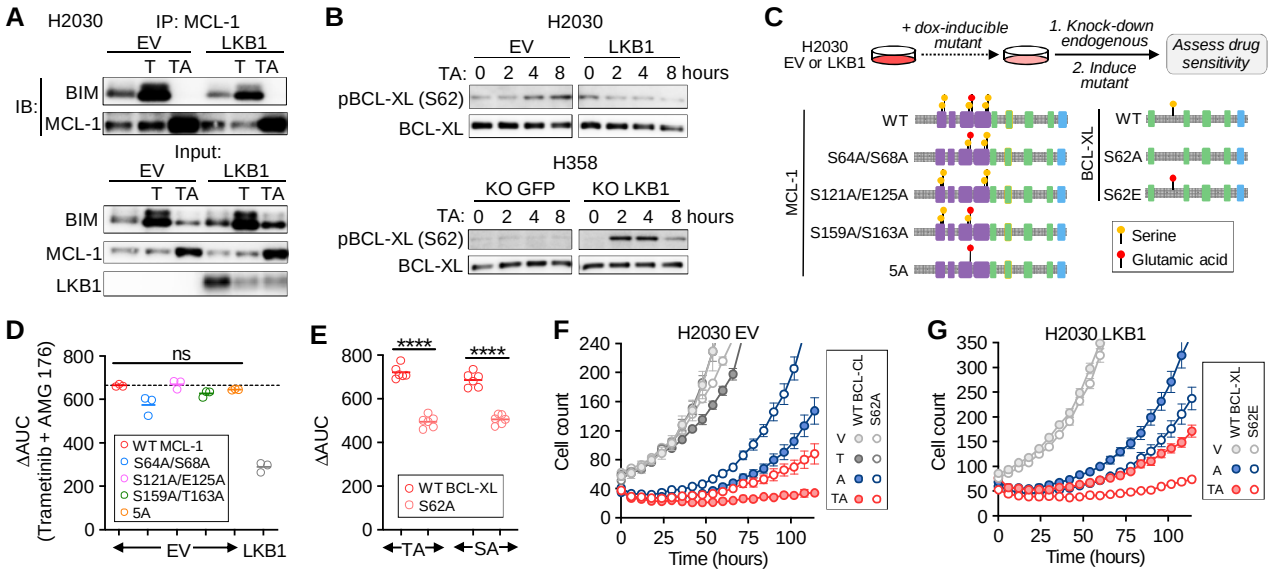

Figure 3. JNK phosphorylates BCL-XL to drive an MCL-1 dependent state. A. Co-Immunoprecipitation of BIM bound to MCL-1 in H2030 EV and H2030 LKB1 cells after treatment with vehicle, trametinib (0.1 μM) for 24 hours or trametinib for 24h followed by AMG 176 (1 μM) for 4 hours. **B.** Time course of BCL-XL S62 phosphorylation in isogenic H2030 and H358 cells by western blot after treatment with 0.1 μM trametinib + 1 μM AMG 176. **C.** Experimental approach for expressing MCL-1 & BCL-XL phospho-site mutants while suppressing endogenous MCL-1 and BCL-XL. Interrogated phosphorylation sites are designated in yellow, phosphomimetic sites in red. **D.** MCL-1 phospho-site mutants do not reduce sensitivity to MCL-1 inhibition (ΔAUC). After induction of mutant MCL-1 (or WT control) and knockdown of endogenous MCL-1, H2030 EV cells were treated with trametinib in the absence or presence of AMG 176 (1 μM) and viability was determined after 3 days. Each dot is an independent biological replicate (N=3). **E.** BCL-XL S62A mutant decreases MCL-1 dependence. After induction of BCL-XL S62A (or WT control) and knockdown of endogenous BCL-XL, H2030 EV cells were treated with sotorasib or trametinib alone or in the presence of AMG 176 (1 μM) and viability was determined after 3 days. Each dot is an independent biological replicate (N=6). **F-G.** H2030 EV cells expressing inducible WT or S62A mutant BCL-XL S62A (F) or H2030 LKB1 cells expressing inducible WT or BCL-XL S62E phosphomimetic (G) were treated with 0.1 μM trametinib or 0.1 μM trametinib in combination with 1 μM AMG 176 and cell number was quantified by live-cell imaging. Data are mean and S.E.M. of 3 technical replicates. V: Veh, T: Trametinib, A: AMG 176, TA: Trametinib + AMG 176.

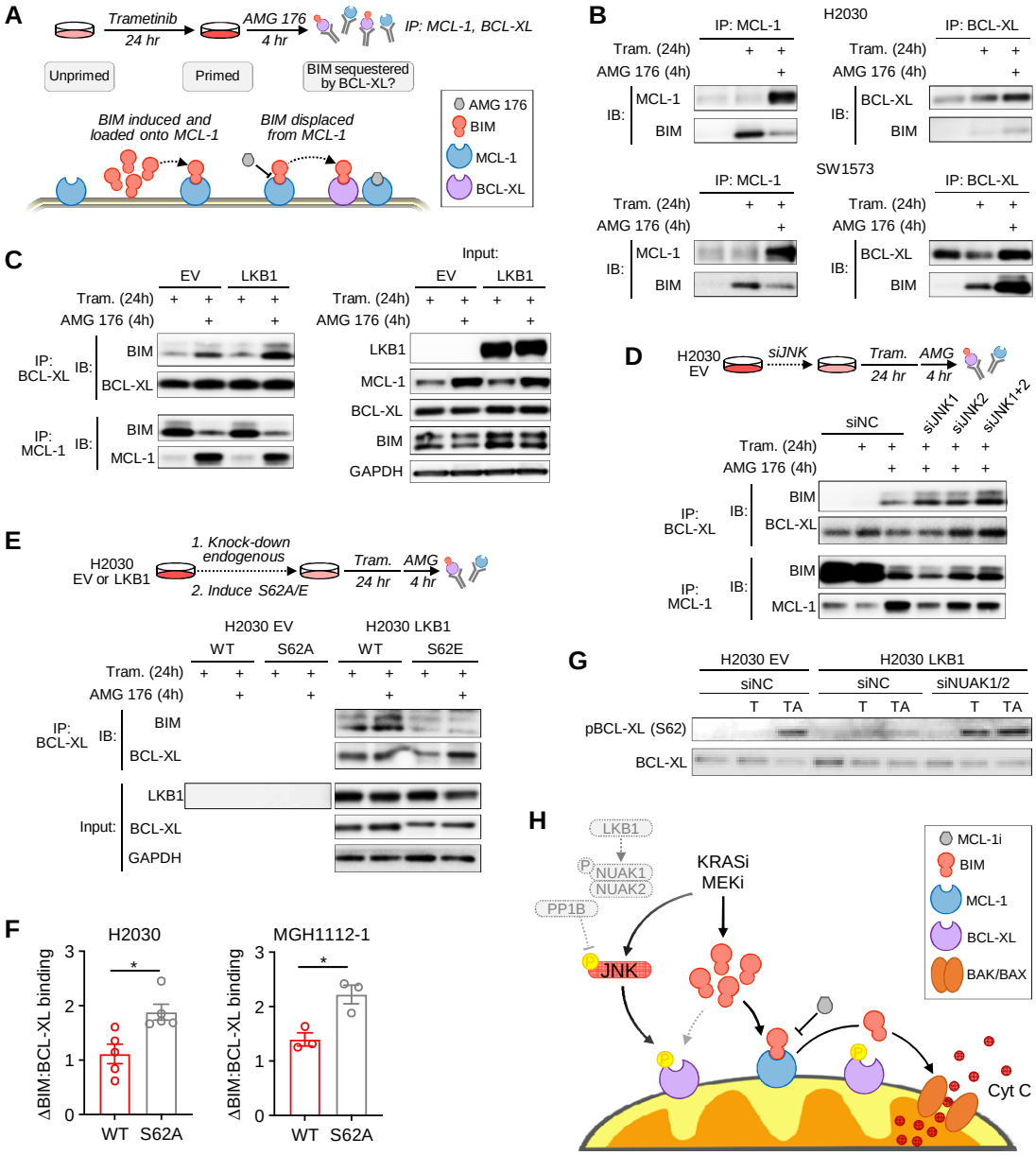

Figure 4. JNK activation drives an MCL-1 dependent state by modulating BIM:BCL-XL interactions. A. Schema for approach to investigating BIM sequestration upon displacement from MCL-1. **B.** Co-IP assessment of BIM bound to MCL-1 and BCL-XL in H2030 (LKB1-deficient) and SW1573 (LKB1 wild-type) cells after treatment with 0.1 μM trametinib for 24 hours followed by 1 μM AMG 176 for 4 hours. **C.** Co-IP assessment of BIM bound to BCL-XL and MCL-1 in H2030 EV and LKB1 cells after treatment with 0.1 μM trametinib for 24 hours followed by 1 μM AMG 176 for 4 hours. **D.** Co-IP assessment of BIM bound to BCL-XL and MCL-1 in H2030 EV with JNK knockdown after treatment with 0.1 μM trametinib for 24 hours + 1 μM AMG 176 for 4 hours. **E.** Co-IP assessment of BIM bound to WT BCL-XL or BCL-XL mutants in H2030 EV (S62A) and H2030 LKB1 (S62E) cells after treatment with 0.1 μM trametinib for 24 hours followed 1 μM AMG 176 for 4 hours. HA-tag pull downs are specific for inducible constructs. **F.** Quantification of Co-IP assessment of BIM bound to BCL-XL in H2030 and MGH1112 cells overexpressing BCL-XL WT or S62A mutants. Data are mean and S.E.M., each dot represents a biological replicate (N=3-5). **G.** Effect of NUAK1/2 knockdown on BCL-XL S62 phosphorylation in response to treatment with 0.1 μM trametinib for 48h (T) or trametinib for 48 hours followed by 1 μM AMG 176 (TA) for 4 hours. **H.** Model depicting the mechanism by which LKB1 loss leads to an MCL-1-dependent state and sensitizes *KRAS*-mutant NSCLCs to combined KRAS or MEK + MCL-1 inhibition**.**

Figure 4

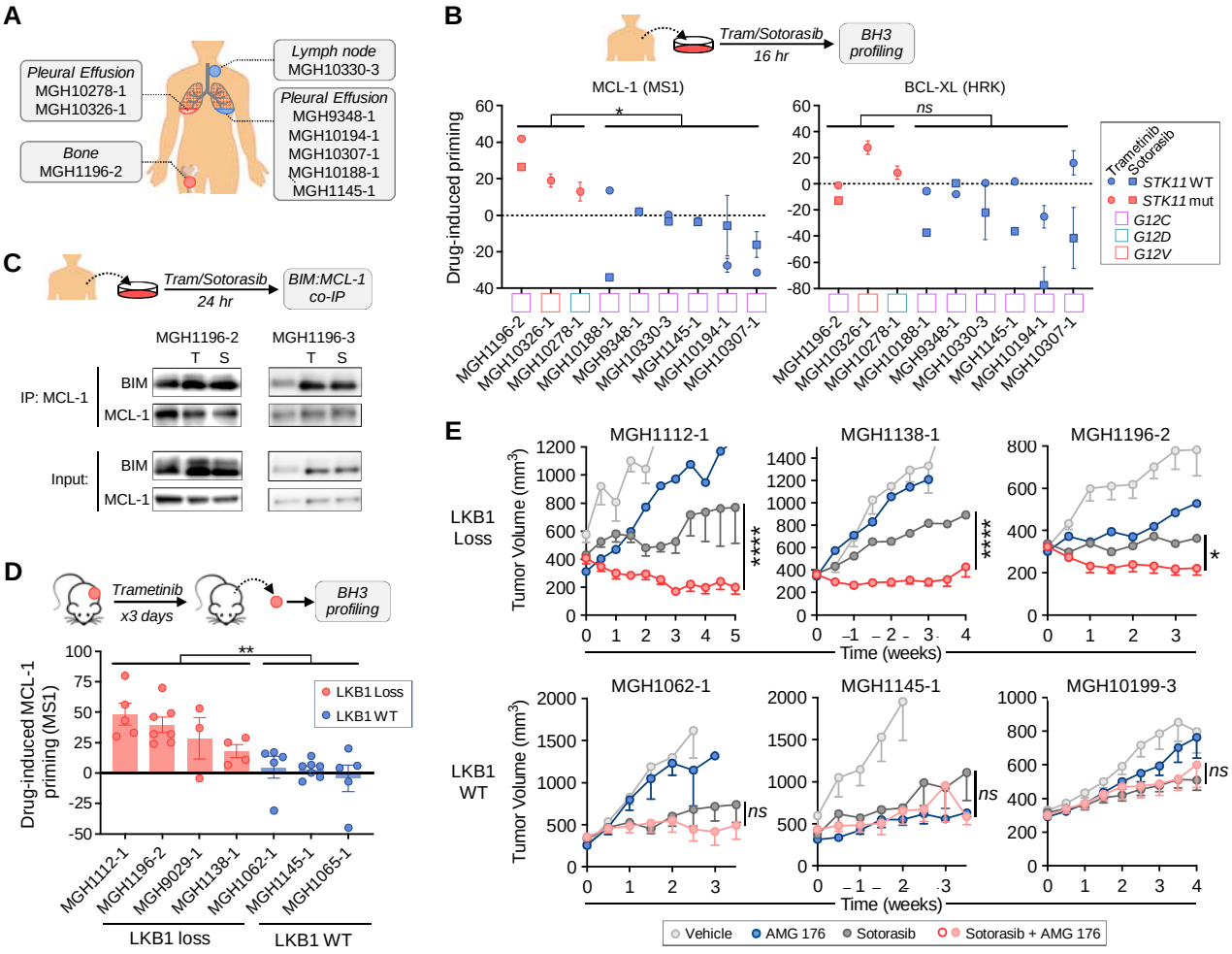

Figure 5. LKB1 loss in associated with MCL-dependence of *KRAS*^{G12C}-mutant NSCLC PDX tumors and patient tumor explants. A. *KRAS*^{G12C}-mutant NSCLC tumor cells were collected for BH3 profiling and assessment of BIM:MCL-1 interactions after *ex vivo* treatment with sotorasib or trametinib. **B.** Change in MCL-1 (MS1 10 + 30 µM peptide) and BCL-XL (HRK 10 + 100 µM peptide) dependent priming of patient tumor cells after *ex vivo* treatment with 0.1 µM trametinib or 1 µM sotorasib treatment. **C.** Co-IP assessment of BIM:MCL-1 interaction in tumor cells isolated from pleural fluid after *ex vivo* treatment with 0.1 µM trametinib (T) or 1 µM sotorasib (S) for 16 hours. **D.** Mice bearing *KRAS*^{G12C}-mutant NSCLC patient derived xenograft (PDX) tumors were treated with sotorasib (100 mg/kg) for 3 days and harvested for BH3 profiling. Data shown is the difference in MCL-1 dependent priming (MS1 peptide) between vehicle and sotorasib treated tumors, each dot represents an independent tumor (N=3-7). **E.** Mice bearing *KRAS*^{G12C}-mutant NSCLC PDX tumors (LKB1-loss: MGH1112-1, MGH1138-1, MGH1196-2; LKB1 WT: MGH1062-1, MGH1145-1, MGH10199-3) were treated with vehicle, sotorasib (100 mg/kg) or sotorasib (100 mg/kg) + AMG 176 (50 mg/kg) daily. Data shown are mean and S.E.M. of N=7-10 animals per arm (**p<0.01, ***p<0.001 as determined by mixed-effects model).

Figure 5